An examination of the kinematics and behavior of mallards (*Anas platyrhynchos*) during water landings

John Gardner Whitehead

Dissertation submitted to the Faculty of the
Virginia Polytechnic Institute and State University
in partial fulfillment of the requirements for the degree of

Doctor of Philosophy
In
Biological Sciences

John J. Socha, Chair
Ignacio Moore
Sunghwan Jung
Shane D. Ross
Jeffrey Walters

May 4, 2020
Blacksburg, VA

Keywords: Mallards, kinematics, flight, landing, Tau Theory, obstacle avoidance

An examination of the kinematics and behavior of mallards (*Anas platyrhynchos*) during water landings

John Gardner Whitehead

Academic abstract

This dissertation aims to address how a change in landing substrate may change landing kinematics. To examine this possibility, mallards (*Anas playtrhynchos*) were used as a study species and 177 water landings were recorded through the use of two camera systems with photogrammetric capabilities. This enabled the landing trajectory and landing transition kinematics to be tracked in three dimensions. From the resulting position data three questions were pursued. Do mallards regulate landing kinematics through a $\dot{\tau}$-constant strategy? With what kinematics do mallards land on water? Do landing kinematics respond to external factors, such as an obstacle to landing? Chapter 2 assesses the presence of a $\dot{\tau}$-constant regulatory strategy and compares the implementation to other landing behaviors. Chapter 3 examines the variation observed in the landing kinematics of mallards, identifies the primary kinematic drivers of that variation, and detects differences in kinematic profile. Chapter 4 inspects the landing kinematics combined with the positions of all other waterfowl in the vicinity to test for the presence of obstacle avoidance behavior.

An examination of the kinematics and behavior of mallards (*Anas platyrhynchos*) during water landings

John Gardner Whitehead

General Audience Abstract

Control of landing is an important ability for any flying animal. However, with the exception of perch landing, we know very little about how birds and other flyers land on a variety of different surfaces. Here, we aim to extend our knowledge in this area by focusing on how mallard ducks land on water. This dissertation addresses the following questions. Do mallards regulate landing speed and trajectory the same way as pigeons? At what speeds, angles, and postures do mallards land on water? Can mallards adjust landing behavior to avoid collisions with other birds on the water surface? Chapter 2 determines how mallards regulate landings and how it is similar and different from pigeons and several other flyers. Chapter 3 describes the speeds, angles, and postures used by mallards to land on water. In addition, this chapter finds evidence for at least two different categories of landing performed by mallards. Chapter 4 provides evidence that mallards avoid situations in which a collision with another bird is likely. However, it is unclear if this is an active choice made by the mallard or due to other circumstances related to the landing behavior. Overall, this dissertation illustrates how the landing behavior of mallards is similar to what has been documented in other animals. However there are significant differences such as higher impact speeds, and shallower angles. Both of which are likely related to the ability of water to absorb a greater amount of the impact forces than a perch or the ground would.

Acknowledgements

I would like to thank all of the people who helped to get me this far. Both of my primary advisors, Jake Socha and John Phillips. You have both supported, guided, and shared in the ups and downs of the many experimental and intellectual avenues we have explored together. All of my committee members past and present who were all open handed with their knowledge, time, and advice: Ignacio Moore, Shane Ross, Sunny Jung, Jeff Walters, Martha Muñoz, and Kendra Sewall. All of my lab mates in both the Socha and Phillips labs. From early-morning and late-night field work, sweating in the sun for snakes, and endlessly clicking on ducks your help and humor through it all has been incredible. All of the undergrads who have volunteered to help trap wild mice, film ducks, and click on wands and ducks; your contributions have been invaluable.

To all of my friends; Dan, Chelsea, Melissa, Eric, and Joel in particular. You have frequently lent an ear to my ramblings about ducks and provided me with the occasional distraction from work I didn't know I needed. To my family, who have always supported me and continue to do so. Your love and support are a constant in my life that is truly a treasure. Last, to my wife. You have endlessly listened, supported, and challenged me. Your love and confidence in me will always inspire me to continually explore and learn about this miraculous world we live in.

Table of Contents

List of Figures & Tables

Chapter 1

The mechanics of flight and landing

1.1 *Introduction*

Powered flight has evolved independently at least four times in history, in pterosaurs, insects, bats, and birds (Templin, 2000). Of these groups, only pterosaurs are extinct, and flight in insects, mammals, and birds has led to an incredible degree of diversification within those taxa, representing over 1.5 million species of insects, 18,000 (Ignacio think 10k more accurate, Jeff prefers more conservative number, less splitting of taxa) species of birds, and 1,400 species of bats (Barrowclough et al., 2016; Burgin et al., 2018; Stork, 2018). The rarity at which flight has evolved, combined with the breadth of diversity within those groups which achieve it, is indicative of the difficulty of evolving the capability of flight, but also of its benefits when achieved. The advantages of flight as a form of locomotion are seen in increases in locomotor speed and efficiency with which an organism can avoid predation, forage, search for mates, and/or migrate (Biewener, 2007). However, flight frequently also comes with higher metabolic costs and strong physical constraints, related to gravity and the density of air (Alexander, 1983; Biewener, 2007).

To fly, an animal must generate enough lift to counteract the force of the their weight, generated by gravity and their mass, and the amount of lift one can generate is inherently dependent upon the density of the air (Alexander, 1983). These constraints on animals have led to a limited number of analogous airfoil structures and kinematics to generate the required lift for flight. The result is that different classes of flying animals can have a high degree of homoplasy in regard to wing form (Ellington, 1991; Rayner, 1988; Templin, 2000). Such homoplasy may be strongest between bats and birds, which fulfill similar aerial niches and have analogous wing structures. However, there are also analogous traits with regards to wing form between insects and the larger vertebrate fliers (Templin,

2000). However, once a basic airfoil has evolved, extant flyers have diversified this basic design into an incredible array of forms which have different chord lengths, spans, and wing loading properties as well as variation in the kinematics in how an animal moves their wing (Dudley, 2002; Ellington, 1991; Evangelista, 2013; Evangelista et al., 2014; Thomas and Taylor, 2001). These shifts in the shape of a flyers airfoil are frequently related to the aerial trade-off of stability or instability, where stability can decrease the energetic cost of flight (gliding) and instability increases maneuverability (Brown, 1963; Thomas and Taylor, 2001).

This tradeoff between stability and instability can be seen in the variation within these taxa as well, and is particularly well documented among birds (Rayner, 1988). Within this large taxonomic group there is an incredible diversity of wing morphology, body shape, and flight behavior. Two examples on the ends of some of these distributions are vultures and chimney swifts. Vultures have long wings compared to their body length, with splayed feathers at the end and a deep chord length, features that make them very efficient at soaring in thermals and provide higher stability, but lower maneuverability. Chimney swifts have smaller wings with extremely tapered tips making them quick and agile, but they are not very effective at soaring or gliding due to this higher maneuverability, but lower stability. Comparisons of such morphologies and their efficiencies, particularly in soaring flight, can be and are continuing to be examined, modeled, and implemented into engineered flyers such as planes or MAVs (Biewener, 2007; Gravish and Lauder, 2018; Lentink, 2017; Norberg, 2002). More challenging, but also beginning to be tackled, are studies breaking down the dynamics involved in active flapping flight that may lead to further innovation in our devices, particularly among drones (Biswal et al., 2019; Lentink, 2014; Lentink, 2017). However, partially due to methodological limitations, most of these studies have focused on steady flight in wind tunnels or short flights from perch to perch that can be controlled in a laboratory. Flyers can perform across a spectrum of aerial conditions other than steady flight and flights from perch to perch. A number of modes of flight are less well studied, two of which are takeoff and

landing (Roderick et al., 2017). In addition, takeoff and landing as flight transitions are unique in that they are maneuvers that must incorporate all the same aerial conditions as other modes of flight, but also the transition to a new substrate – solid or fluid. Birds demonstrate an ability to takeoff and land from solid flat surfaces (the ground or walls), solid and pliable cylinders (branches of varied size), and fluids (water) (Roderick et al., 2017; Roderick et al., 2019). Understanding how birds move and control these flight transitions, and how changes in substrates may change the kinematics or control methods, may be an important additional source of bioinspiration and biomimetic design from which to design and control more versatile man-made drones.

This dissertation aims to examine implication of water as a landing substrate. Water was chosen due to the fact that it is physically different, as all other substrates bird are known to land on are solid, even if they vary in shape and pliability. Water also presents different advantages and challenges as a landing substrate. An advantage of water is its compliance compared to solid substrates. As a fluid, at comparative velocities water is more effective at absorbing kinetic energy than a solid substrate (Alexander, 1983). This means the reaction forces from impact upon the bird at landing will be less than if it landed with the same kinematics on a solid substrate. However, water also introduces new challenges. When landing on a perch in particular, a bird can effectively grasp the substrate to help brake and maintain balance while landing (Roderick et al., 2019). In water, the substrate is another fluid, so grasping is futile. Instead, as the feet and other parts of the bird make contact with the water those surfaces will generate additional forces of lift and drag; these forces may also be further complicated by wave drag due to the interactions at the air-water interface (Alexander, 1983; Lovvorn et al., 2001; Zhan et al., 2017). A bird must be able to maintain balance throughout the changing torques that are generated by fluid dynamics during a landing.

In addition to these physical characteristics of the substrate, there is variation among birds that land on water in their qualitative kinematics. Prior to this dissertation, the only examination of how

birds land on water was on red-throated loons (*Gavia stellata*) (Norberg and Norberg, 1971), and detailed kinematics are absent from the study due to limitations of the camera technology and photogrammetric techniques at the time. However, loons specifically land on their breast, which appears to be unique to this group of waterfowl (Norberg and Norberg, 1971). With the exception of diving behaviors – which are excluded from this work as they are motivationally and kinematically distinct from landing behavior – all other birds that land on water appear to do so feet-first, which is similar to other landing behaviors seen in birds. Therefore, to begin examining the kinematics and behavior of water landing, mallards (*Anas* platyrhynchos) were chosen as a study system. Mallards preferentially land on water in the more commonly seen feet-first style. In addition, they are ubiquitous across the northern hemisphere (Kulikova et al., 2005) and already represent a significant presence as a study species within other fields of literature – including a few in biomechanics where there have been several studies on swimming (Aigeldinger and Fish, 1995; Clark and Fish, 1994) and an analysis on the wing aerodynamic properties (Dial et al., 2012).

The aims of this dissertation are threefold: i) to examine how mallards regulate the kinematics with which they land on water, ii) to quantify the kinematics with which mallards land on water, and iii) determine whether landing behavior shifts in response to an external factor, specifically the presence or absence of other duck in the landing vicinity. Understanding these three aspects of how mallards land on water will establish what the kinematics are with which ducks land on water, how those kinematics are detected and thereby regulated, and if the landing behavior has some degree of plasticity enabling it to adapt to changing conditions.

1.2 *References*

Aigeldinger, T. and Fish, F. (1995). Hydroplaning by ducklings: overcoming limitations to swimming at the water surface. *J. Exp. Biol.* **198**, 1567–74.

Alexander, R. M. (1983). Motion in fluids. In *Animal mechanics*, pp. 183–236. Funtington: Blackwell Scientific Publications.

Barrowclough, G. F., Cracraft, J., Klicka, J. and Zink, R. M. (2016). How many kinds of birds are there and why does it matter? *PLoS One* **11**, 1–15.

Biewener, A. A. (2007). Movement in air. In *Animal Locomotion* (ed. Willmer, P.) and Norman, D.), pp. 111–150. Oxford: Oxford University Press.

Biswal, S., Mignolet, M. and Rodriguez, A. A. (2019). Modeling and control of flapping wing micro aerial vehicles. *Bioinspir. Biomim.* **14**, 026004.

Brown, R. (1963). The flight of birds. *Biol. Rev.* **38**, 460–489.

Burgin, C. J., Colella, J. P., Kahn, P. L. and Upham, N. S. (2018). How many species of mammals are there? *J. Mammal.* **99**, 1–14.

Clark, B. D. and Fish, F. E. (1994). Scaling of the locomotory apparatus and paddling rhythm in swimming mallard ducklings (Anas platyrhynchos): Test of a resonance model. *J. Exp. Zool.* **270**, 245–254.

Dial, T. R., Heers, A. M. and Tobalske, B. W. (2012). Ontogeny of aerodynamics in mallards: comparative performance and developmental implications. *J. Exp. Biol.* **215**, 3693–3702.

Dudley, R. (2002). Mechanisms and implications of animal flight maneuverability. *Integr. Comp. Biol.* **42**, 135–140.

Ellington, C. P. (1991). Limitations on animal flight performance. *J. Exp. Biol.* **160**, 71–91.

Evangelista, D. J. (2013). *Aerial righting, directed aerial descent, and maneuvering in the evolution of flight in birds.* Doctoral. University of California, Berkley.

Evangelista, D., Cam, S., Huynh, T., Kwong, A., Mehrabani, H., Tse, K. and Dudley, R. (2014). Shifts in stability and control effectiveness during evolution of Paraves support aerial maneuvering hypotheses for flight origins. *PeerJ* **2**, e632.

Gravish, N. and Lauder, G. V. (2018). Robotics-inspired biology. *J. Exp. Biol.* **221**, jeb138438.

Kulikova, I. V., Drovetski, S. V., Gibson, D. D., Harrigan, R. J., Rohwer, S., Sorenson, M. D., Winker, K., Zhuravlev, Y. N. and McCracken, K. G. (2005). Phylogeography of the Mallard (Anas Platyrhynchos): Hybridization, dispersal, and lineage sorting contribute to complex geographic structure. *Auk* **122**, 1309.

Lentink, D. (2014). Bioinspired flight control. *Bioinspiration and Biomimetics* **9**,.

Lentink, D. (2017). Coevolving advances in animal flight and aerial robotics. *Interface Focus* **7**, 6.

Lovvorn, J. R., Liggins, G. a, Borstad, M. H., Calisal, S. M. and Mikkelsen, J. O. N. (2001). Hydrodynamic drag of diving birds : Effects of body size, body shape and feathers at steady speeds. *J. Exp. Biol.* **1557**, 1547–1557.

Norberg, U. M. (2002). Structure, form, and function of flight in engineering and the living world. *J. Morphol.* **252**, 52–81.

Norberg, R. Å. A. and Norberg, U. M. (1971). Take-off , landing , and flight speed during fishing flights of *Gavia stellata*. *Ornis Scand.* **2**, 55–67.

Rayner, J. M. V. (1988). Form and function in avian flight. *Curr. Ornithol.* 1–66.

Roderick, W. R. T., Cutkosky, M. R. and Lentink, D. (2017). Touchdown to take-off: at the interface of flight and surface locomotion. *Interface Focus* **7**, 20160094.

Roderick, W. R., Chin, D. D., Cutkosky, M. R. and Lentink, D. (2019). Birds land reliably on complex surfaces by adapting their foot-surface interactions upon contact. *Elife* **8**, 1–23.

Stork, N. E. (2018). How many species of insects and other terrestrial arthropods are there on earth? *Annu. Rev. Entomol.* **63**, 31–45.

Templin, R. J. (2000). Spectrum of animal flight: Insects to pterosaurs. *Prog. Aerosp. Sci.* **36**, 393–436.

Thomas, A. L. R. and Taylor, G. K. (2001). Animal flight dynamics I. Stability in gliding flight. *J. Theor. Biol.* **212**, 399–424.

Zhan, J. M., Gong, Y. J. and Li, T. Z. (2017). Gliding locomotion of manta rays, killer whales and swordfish near the water surface. *Sci. Rep.* **7**, 1–12.

Chapter 2

Mallard duck landing behavior follows a $\dot{\tau}$-constant braking strategy

Abstract

Many flying animals use optic flow to control movement through the air, including during landing maneuvers. In particular, pigeons, hummingbirds, bats, *Draco* lizards, and bees demonstrate the use of the $\dot{\tau}$ constant braking strategy when landing. This regulatory strategy implies an animal regulates its approach to an object through keeping the rate of change of the relationship between the distance to an object and the rate of change of that distance constant. In keeping this ratio, τ, constant a variety of deceleration profiles can be generated that can lead to different collision avoidance behaviors. The landing behaviors listed above all qualify as controlled collisions, in which the animal is decelerating into the object. This study examines whether the same regulatory strategy is employed by mallards to land on water to assess if a change in landing substrate requires a change in regulatory strategy. Video of landing behavior of mallards was recorded at a local pond and digitized (N=177), which enabled kinematic and τ parameters to be calculated for each landing. It was found mallards do employ this $\dot{\tau}$-constant strategy, having a Pearson linear coefficient for τ with respect to time to land with a mean and standard deviation of 0.99 ± 0.02. This implies regulation by the birds to fix $\dot{\tau}$ at a constant while landing. The values of $\dot{\tau}$ observed in mallards were higher than the other animals when doing landing behaviors. Mallards tend to maintain a $\dot{\tau}$ of 0.90 ± 0.13, while those of other three powered flight landing animals (pigeons, hummingbirds, and bats) maintain a $\dot{\tau}$ of 0.775 ± 0.109, 0.710 ± 0.132, and 0.702 ± 0.052. The only gliders, *Draco* lizards, maintain a higher $\dot{\tau}$, but still lower than the mallards at 0.84 ± 0.08. This higher $\dot{\tau}$ maintained by mallard may be indicative of the change in substrate from solid branches and trunks for the other flyers to water for the mallards. The increased compliance of the water in comparison to a solid substrate may enable the mallards to let the water absorb impact forces that could be injurious on a solid substrate. Therefore, the mallards are braking less through slow, flapping flight to expend less energy for landing.

2.1 *Introduction*

One challenge flying animals face is how to regulate and control landing approach kinematics to avoid a potentially dangerous collision. This necessitates that the animal can detect its own self-movement through an environment. For insects and birds vision is the primary system through which spatial information is processed and optic flow is the primary visual cue used to detect self-movement (Altshuler and Srinivasan, 2018). Optic flow is how quickly position of objects and patterns on the retina shifts; it is this cumulative rate of change that enables an organism to detect a relative measure of how quickly they are moving with respect to the environment (Gibson, 1958; Koenderink, 1986). Since its discovery, optic flow has been demonstrated as essential to how birds (Bhagavatula et al., 2011; Dakin et al., 2016; Vo et al., 2016) and insects (Baird et al., 2013; Chakravarthi et al., 2018; Linander et al., 2015; Srinivasan et al., 1996; Taylor and Krapp, 2007; Wang et al., 2017) detect self-movement in flight. Yet, while optic flow explains how a subject's movement and position relative to their surroundings can be tracked, it does not explain how an organism regulates the information derived from optic flow to navigate its environment.

One proposed theory for regulating optic flow is based on a parameter tau (τ) (Lee, 1976). Tau theory posits that by changing behavior with respect to the ratio τ, defined as the distance to the point of collision over the rate of change of that distance (relative approach velocity to collision), collision behavior can be safely controlled (Lee, 1976; Lee et al., 2009).

$$\tau = x/\dot{x} \tag{1}$$

Where x is the distance to the object and $\dot{x}$ is the rate of change of that distance (Lee, 1976; Lee et al., 2009). Lee proposed that if the rate of change of τ was kept constant, different values of this rate of change ($\dot{\tau}$) could create a variety of different braking strategies and collisions outcomes (Lee, 1976; Lee et al., 2009). This potential collision strategy was termed the $\dot{\tau}$ constant braking strategy (Lee, 1976; Lee et al., 2009).

$$\dot{\tau} = C \tag{2}$$

When modeled, if $\dot{\tau}$ is held constant it creates specific kinematic profiles with respect to velocity and acceleration, which result in several different categories of collision behavior (Fig. 2.1) (Lee et al., 2009).

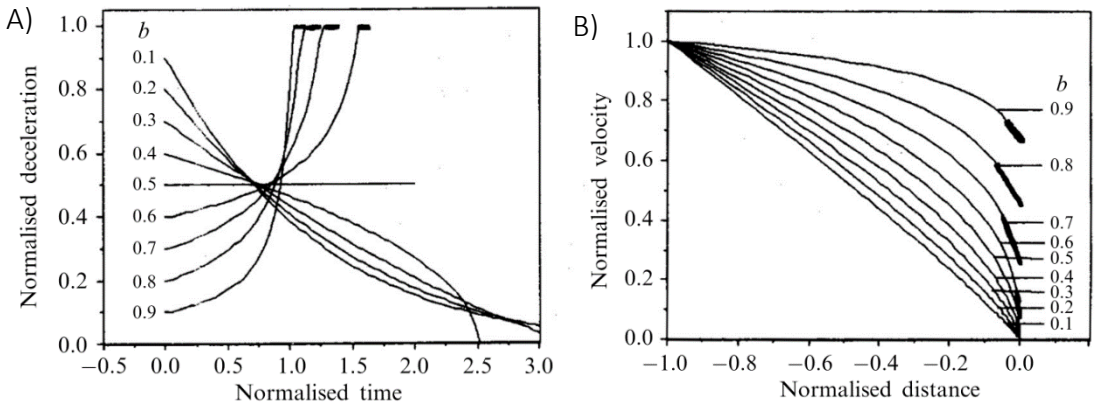

Figure 2.1: The resulting kinematic profile for deceleration with respect to time (A) and velocity with respect to distance (B) assuming a constant $\dot{\tau}$, or braking constant, of 0.1 through 0.9 during a given approach (figure from Lee et al., 2009).

There is a distinct shift at $\dot{\tau}$ = 0.5 with regard to deceleration profiles which enables a broader categorization of these collision behaviors based on $\dot{\tau}$ (Lee et al., 2009). Behaviors with a $\dot{\tau}$ of 0.5 or less, will barely reach the object or be short, considered as a collision-avoidance behavior (Lee, 1976). If $\dot{\tau}$ is greater than 0.5 and less than 1, collision will occur, but braking is increasing before impact, considered as a controlled collision (Lee, 1976). Lastly, if $\dot{\tau}$ is greater than 1, the subject will accelerate into the collision (Lee, 1976).

Evidence for a visually regulated constant braking strategy has been demonstrated in flying animals such as pigeons landing on a perch (Lee et al., 1993), hummingbirds approaching a feeder (Lee et al., 1991), lizards gliding to trees (Khandelwal and Hedrick, 2020), and bees landing (Baird et al., 2013). In addition, a constant braking strategy has been demonstrated in bats landing on a hand (Lee et al., 1995). Though this behavior is likely regulated by echolocation as opposed to vision, the landing kinematics follow a similar $\dot{\tau}$ constant braking strategy with distance and relative velocity detected by the animal through a different sensory system. Pigeons, hummingbirds, Draco lizards, and bats all carried out these approach behaviors with a mean $\dot{\tau}$ and standard deviation of 0.775 ± 0.109, 0.710 ± 0.132, 0.84 ± 0.08, and 0.702 ± 0.052 respectively. These values of $\dot{\tau}$ categorize these three behaviors as controlled collisions (Lee, 1976). This makes intuitive sense, as while these are different behaviors in different species, all are movement to object behaviors in which the subject needs to make contact with the object. Therefore, an approach strategy where the subject increasingly decelerates up to the point of contact would be expected.

However, one feature of landing on a trunk, perch, or feeding from a flower is that the point of impact with the object is relatively small. If landing occurs on a larger surface, such precision in the point of landing may not be required. Furthermore, water as a landing substrate is much more compliant than the solid substrates examined in the previous studies. The influence of compliance of substrates on gait is well established (McMahon, 1985) and animals such as goats actively adjust limb stiffness to compensate for changes in substrate compliance (Clites et al., 2019). Landing on the more compliant surface of water and in a way that contacts a greater length of the substrate may require different values of $\dot{\tau}$ or a different regime for how optic flow is regulated altogether. Here, we examine water landings to test if the $\dot{\tau}$ constant strategy is still employed when a bird lands with higher velocities and in

a situation where the landing point may be more less precise. If so, does the value of $\dot{\tau}$ shift significantly from what has previously been documented for birds? To do this we examined how mallard ducks (*Anas platyrhynchos*) land on water. Mallards, when landing on water, frequently impact with high velocity and skim past the point of impact making it plausible mallards' $\dot{\tau}$ constant strategy is different then what has been documented in previous landing behaviors.

2.2 *Methods*

Landing trajectories of mallard ducks (*Anas platyrhynchos*) were recorded at a local pond in Blacksburg, VA, United States. The pond, is typically inhabited by a mixed flock of multiple species of waterfowl, largely comprised of a residential population of mallard ducks. Point counts were carried out at four locations (Fig. 2.2A), the site of filming and three other locales in the vicinity of the filming location (filming cove). The three sites were a gazebo on the far side of the same pond filming was done, a neighboring pond which drains into the filming pond (small duck pond), and the edge of the

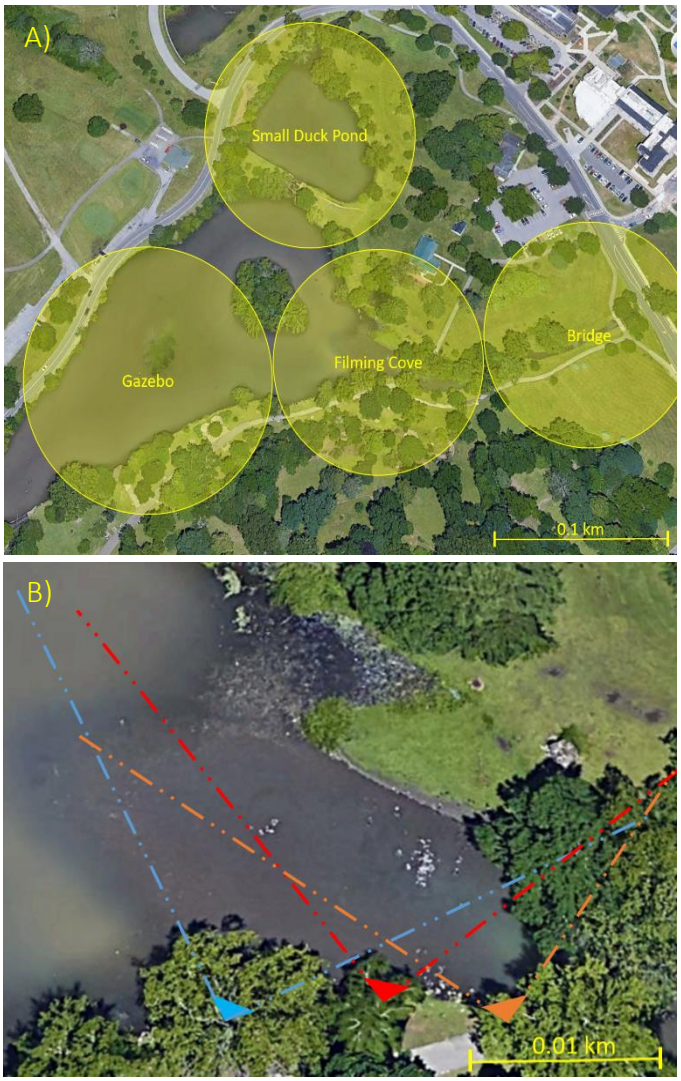

Figure 2.2: The site of filming and camera placement. A larger scale view of the park in which filming was done and the four point count regions (A) used to measure the population of mallards that were being filmed. The arrangement of cameras along the shore where filming was done (B). Each triangle is a camera placement and the dashed lines represent the approximate view that camera has of the volume of interest (VOI).

park by the creek which drains into the pond (bridge). Each site was visited for 10 minutes and a count was taken for any waterfowl in the water or within 15 meters of the water, water includes the creek which flows down into the filming cove for the bridge count location. All of these regions are areas waterfowl could be found and where groups were known to make flights into the filming area. A variety of species are present at this pond and some migratory groups of mallards use the pond some of which stay to breed. However, a significant number of the Mallards are residential. Counts showed that from March 2018 to February of 2019 there was a mean and standard deviation of 56 ± 24 mallards present between these four locales (Fig. 2.3A). However, due to additional migrants and movement of birds throughout the year that population fluctuated substantially, but never dropped below 30 (Fig 2.3B).

To record landings, three videocameras (HERO4 Black, GoPro, Los Angeles, CA, USA), on wide view at 4k and 30 fps were placed along one segment of the shore with a spacing of approximately 3-5 meters between each camera. The videocameras were each placed on a tripod, with the camera approximately 30-50 cm above the ground and pointed towards the volume of interest (VOI) (Fig. 2.2B). A remote control (WiFi Smart Remote, GoPro, Los Angeles, CA, USA) was used to start recordings from all 3 cameras when a landing event was about to occur. Lastly, radios were attached to each tripod with a 4th held by the recorder so a tone could then be pulsed 3 times by the recorder from the radio and that tone would emit at the radios on each tripod (Jackson et al., 2016). This method of post-hoc synchronization, using exterior temporal cues such as light or sound pulses for synchronization, limits the time shift of tone detection on the audio track in comparison to emitting a tone from a single radio

increasing the accuracy of the post-hoc synchronization of any given recording (Jackson et al., 2016).

Filming occurred sporadically for a total of 26 days in December 2016 to March of 2017, and October 2018 to February 2019. Landings from a recording were only analyzed if the local wind speed was below 5.4 m/s on a handheld anemometer (WM-2 Ambient Weather handheld weather meter, Chandler, AZ, USA), classified as a gentle breeze on the Beaufort wind scale (The Meteorological Glossary, 1961). This value was chosen based on a previous study, which found that landing waterfowl do not show a directional preference in relation to wind direction below wind speeds of 5.4 m/s (Hart et al., 2013). From the 26 days of filming there are 10 in which the weather conditions were suitable and landing events occurred, during which the highest recorded wind speed was 2.6 m/s. During those 10 days, 244 landings were recorded.

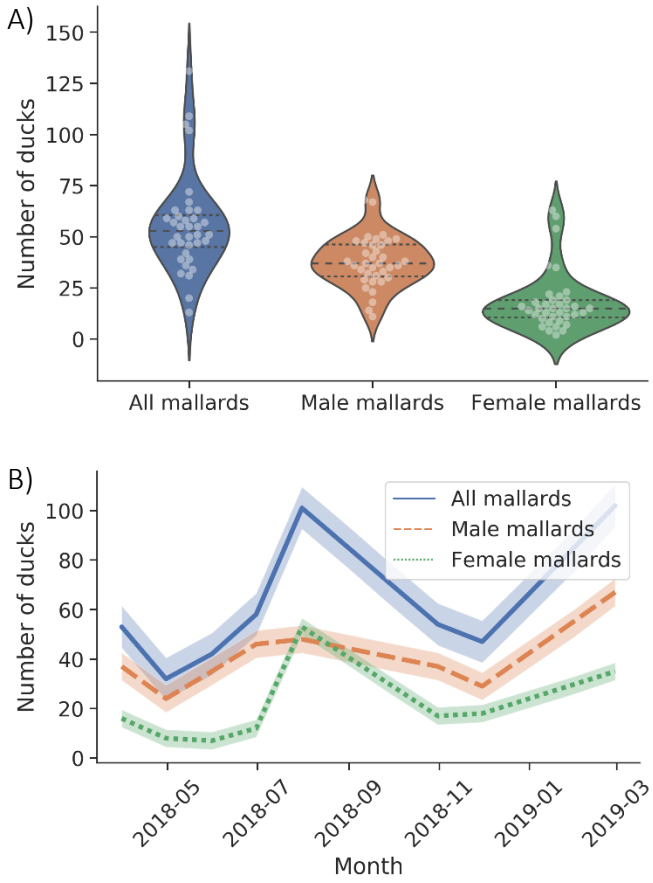

Figure 2.3: Number of ducks from point counts, cumulatively and temporally. The number of mallards observed during point counts within the pond vicinity (A). The average number of all mallards counted was 56 ± 24 (blue), male only was 38 ± 12 (orange), and female only was 18 ± 15 (green). The same point count data for all mallards is plotted temporally by the average count for each month (B). There is fluctuation in the population temporally around periods of migration where the resident population likely experiences an influx of transients. However, the average count per month does not drop below 32 ducks.

Landing videos were processed by de-warping, which removes image distortion of the fish-eye lens of the camera, through Argus software utilizing omnidirectional coefficients (Jackson et al., 2016; Scaramuzza et al., 2006a). Each grouping of 3 videos, one from each camera, was synced based on the series of three tones on the audio tracks (Jackson et al., 2016). Then, the VOI was calibrated through manual digitization of a 0.94 m wand moved through the landing area of the pond. The digitization was done by digitizing a wand every 10 frames until wand points all along the breadth of the VOI were obtained, giving all calibrations greater than 100 wands. From those points direct linear transformation (DLT) coefficients were obtained (Jackson et al., 2016; Zhang, 2000). The maximum variance seen in wand length for a given digitization was ±2.18 cm, which gives a measure of the uncertainty for a given digitization. This variance was considered reasonable for this study as the intended target for digitization is the movement of the whole mallard as a single point and the length of the bill of a mallard is approximately 4 cm (Johnsgard, 2010).

The corresponding DLT coefficients were applied to landing videos where the point at which the neck meets the body was digitized on each mallard in each of the three videos. From those points and the DLT coefficients the 3D points of each landing were calculated(Jackson et al., 2016; Zhang, 2000). After landing digitization two landings were removed because the ducks landed on the ground and an additional 65 landings were removed due to an inability to reliably digitize where the neck meets the body during impact, a key transition point in the landing trajectory. These difficulties frequently arose from the distance or orientation of the subject during impact relative to the cameras and occasionally due to obstruction of the view

by another duck. The gaps in the remaining 177 landings were interpolated using an unscented Kalman filter and then smoothed using a 2nd order Butterworth filter (Yu et al., 1999).

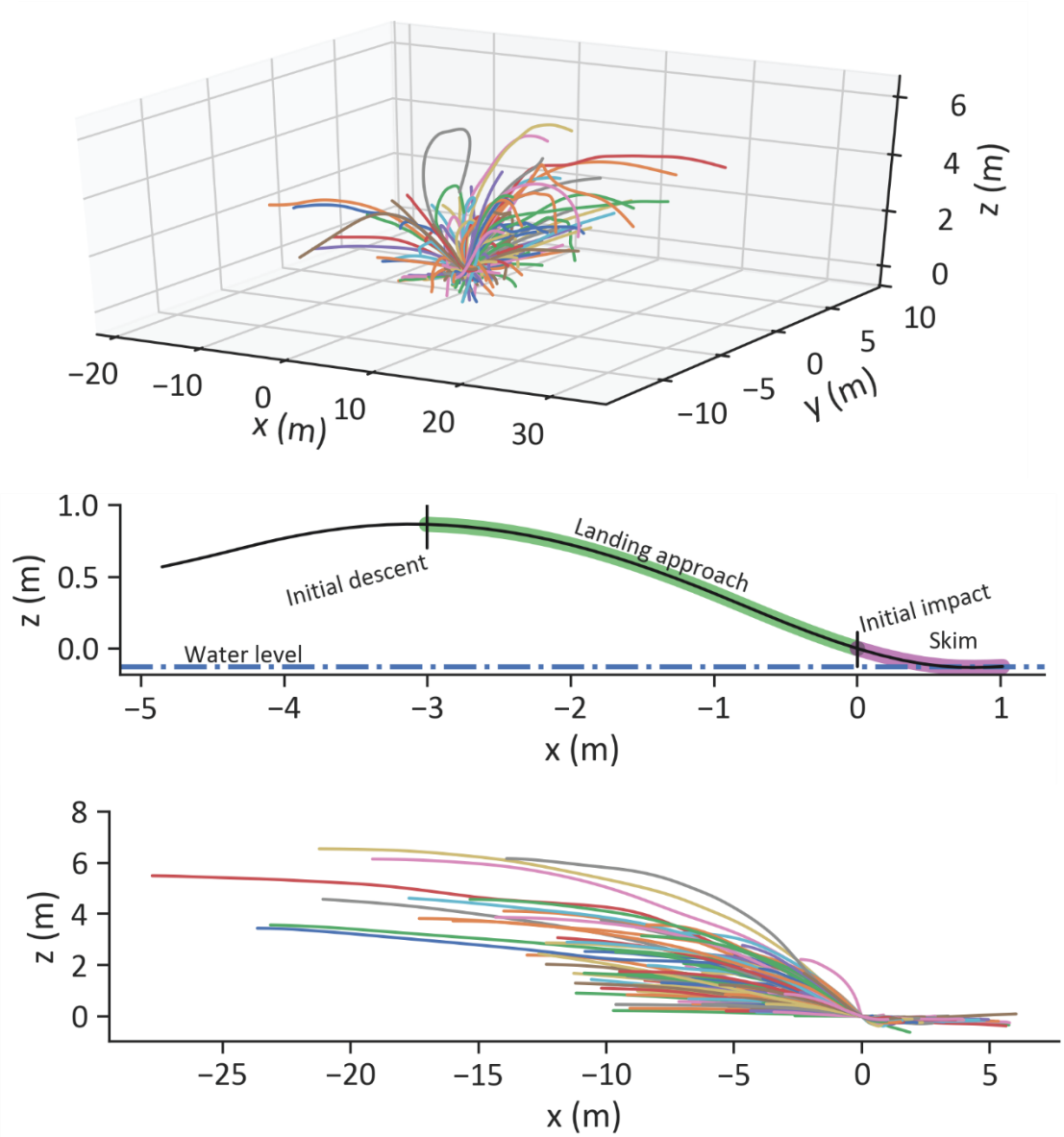

Figure 2.4: Resulting tracking data from digitization and the transformations and selections done to make the landing data more comparable. Once all 177 landing trajectories had gaps interpolated with a Kalman filter and the trajectories smoothed using a Butterworth filter the resulting landings still approached and landed from a variety of directions making comparisons difficult (A). Therefore, the trajectories were straightened into two dimensions, aligned with the initial point of impact for each duck at 0, and the beginning of the landing approach was set as the initial point of descent. This enables each landing to be split into three distinct phases: the landing approach (green), the moment of impact, and the resulting skim after impact (purple) (B). The resulting trajectories after straightening, alignment to impact, and selection of landing approach creates a representation of the data that is easier to compare (C).

The resulting landing trajectories were scattered in 3D space (Fig. 2.4A). To be able to visually compare the trajectories, they were aligned using a custom python code, effectively rotating the trajectories so that all the movement is contained within one horizontal axis and one vertical axis. This code makes the initial vector of a given trajectory the origin. Then, the tracked points are iteratively rotated in the x and y plane until they are in line with the initial vector. Once the landings were spatially aligned, the trajectories were temporally aligned so that the moment of initial impact was zero. Instantaneous velocities for each trajectory were calculated using the finite element derivative of position. Once the landings were straightened into two dimensions, the trajectories were temporally aligned so that the moment of initial impact was zero. Then, the start of each landing sequence was defined by the point of initial descent (Fig. 2.4B). Initial descent was defined as the initial point of negative velocity on the gravity axis observed from the bird. Initial descent was defined to exclude flight behavior in which the bird is not descending and therefore, likely has not begun to land. The described processing enabled each landing to be broken down into a landing approach and skim phases in addition to identification of the moment of initial impact (Fig. 2.4B).

After this processing, $\tau = x/\dot{x}$ was calculated where x is the distance from the location of impact, and $\dot{x}$ is the horizontal velocity at each moment in time. Each landing's individual τ was plotted with respect to time and the Pearson linear coefficient was calculated for each individual trajectory. The rate of change of τ for a given landing, $\dot{\tau}$, was defined as the slope of the linear line of best fit for each trajectory, as in Lee et al. (1993).

Several additional kinematic features of the landings were calculated. Impact speed was calculated as the magnitude of the straightened velocities in both the x and z direction at the

point of initial impact. Trajectory angle at each point in time was calculated as the angle of the resultant velocity vector from the straightened velocity vectors in the x and z direction. Mean approach angle for landing was defined as the mean angle of all the trajectory angles from a landing up to the point of impact. Distance traveled is the total displacement of the bird while it skimmed, defined as the point of impact until the duck performs a behavioral tail waggle and/or wing rearrangement. These behaviors were observed to occur after the bow wave on the breast of skimming ducks diminishes, but are much more visible than the bow wave itself.

2.3 *Results*

From 177 trajectories, ducks landed with an impact speed of 5.0 ± 1.4 m/s (mean and standard deviation). The mean approach angle had a mean of 8.6 ± 6.3 degrees. The trajectory angle at the point before initial impact was 14.8 ± 10.0 degrees. The distance traveled after the point of impact was 2.2 ± 1.3 m. Combined, the kinematics suggest a generalized landing profile that has a gradual approach, with few sudden changes in trajectory, but impacts the water at a high velocity with a shallow angle. This results in a long skim across the water after impact of, on average, over 3 body lengths (measured from tip of bill to base of tail) (Johnsgard, 2010).

With regards to the presence of a $\dot{\iota}$ constant strategy, the Pearson linear coefficients for all landings was 0.99 ± 0.01, with a $\dot{\iota}$ of 0.90 ± 0.13 (Fig. 2.5A). This indicates a strong preference for linearity suggestive of maintaining a constant $\dot{\iota}$ during a landing and to do so following a controlled collision value for $\dot{\iota}$. In addition, a subset of landings in the data, 32, have $\dot{\iota}$ greater than 1, suggesting these individuals are not decelerating into the water but accelerating or in the case of being close to a $\dot{\iota}$ of 1, holding velocity near constant. Therefore, a Mann Whitney U-test for independence in impact speed, impact angle, approach angle, or distance after impact was used to test whether this is a distinct

behavior from the other recorded landings. Of the 32 landings with $\dot{\tau}$ greater than 1, $\dot{\tau}$ was 1.09 ± 0.10 and the Mann Whitney U-Test found only approach angle out of the four kinematic metrics to be statistically different from the distribution from the other landings (p-value < 0.01). Those landings with a $\dot{\tau}$ greater than 1 have an approach angle of 6.9° ± 7.5° while the landings with a $\dot{\tau}$ below 1 have slightly higher approach angle of 8.9° ± 6.0°.

2.4 *Discussion*

The high level of linear correlation shown by the Pearson linear coefficient scores (0.99 ± 0.01) between τ and time to impact strongly supports the hypothesis that mallards use a $\dot{\tau}$ constant braking strategy when landing on water. In addition, the mean value of $\dot{\tau}$ is 0.90 ± 0.13 which follows the prediction of τ theory that landing behavior is a controlled collision and therefore should have a $\dot{\tau}$ between 0.5 and 1.0 (Lee, 1976). The 32 landings with a $\dot{\tau}$ greater than 1 are consistently associated with shallower approaches which, combined with less braking may represent a strong skimming behavior or strategy for landing on water. However, the lack of significant differences in the kinematics in impact speed, impact angle, or distance after impact runs counter to this idea. Instead these lower angle approaches may reflect shorter flights in the dataset in which the individuals do not land with as much control or precision. However, further studies will be needed to assess such potential differences in the control or precision between landings observed here.

Compared to other flyers the presence of a $\dot{\tau}$ constant braking strategy is consistent with what has been seen in pigeons (*Columbia livia*) landing on a perch (Lee et al., 1993), big brown bats (*Eptesicus fuscus*) landing on a hand (Lee et al., 1995), and sparkling violet-ear hummingbirds (*Colibri corsucans*) approaching a feeder (Lee et al., 1991) (Fig. 2.5). Yet, the $\dot{\tau}$ values mallards land on water at appear to be greater than the values documented in these other landing behaviors. Pigeons were found to have a mean $\dot{\tau}$ of 0.775 ± 0.109 (Lee et al., 1993), bats were recorded with a mean $\dot{\tau}$ of 0.702 ± 0.052 (Lee et al., 1995), and hummingbirds

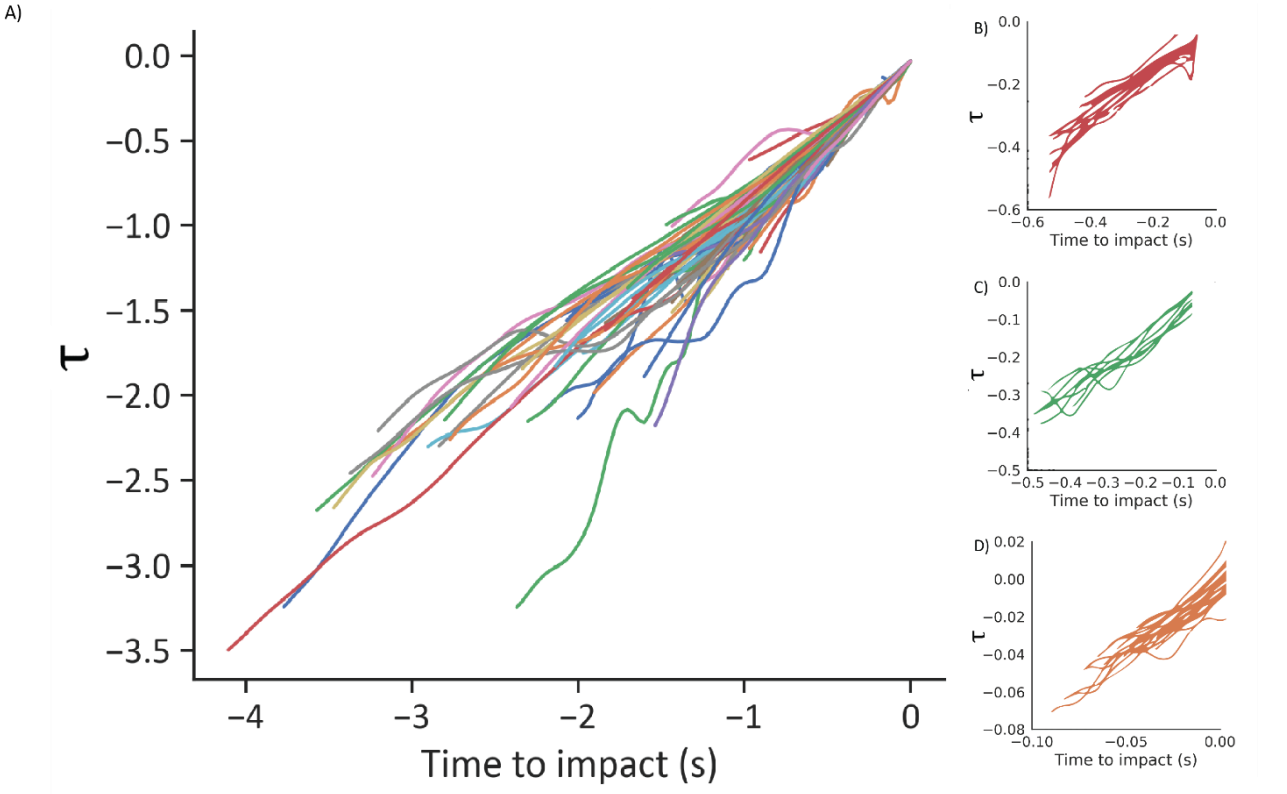

Figure 2.5: The τ for each mallards' landing approach with respect to time until impact (A). Each line represents one landing (N = 177) and the τ that individual has at each point in time based on the distance to initial impact and horizontal velocity at that moment. Recorded landings are different lengths, but there is a general and highly significant trend of linearity for τ in the landing trajectories. For all the landings the mean Pearson Linear Coefficient = 0.99 ± 0.02. To the right and in red are the values of τ found for pigeons (*Columbia livia*) landing on a perch by Lee et al., 1993 (B). In green is the τ found for big brown bats (*Eptesicus fuscus*) landing on a hand by Lee et al., 1995 (C). In orange is the τ found for hummingbirds (*Colibri corsucans*) approaching a feeding tube by Lee et al., 1991 (D). All of these studies demonstrate a linear behavior of τ in support of the utilization of a $\dot{\tau}$ constant braking strategy.

approached at a mean $\dot{\tau}$ 0.710 ± 0.132 (Lee et al., 1991). The mallards were higher at 0.90 ± 0.13.

This upward shift in $\dot{\tau}$ also exceeds that seen for a gliding animal, Draco lizards, which maintain a $\dot{\tau}$ at 0.84 ± 0.08 (Khandelwal and Hedrick, 2020). Arboreal gliders, such as the Draco lizard and flying squirrel, use a stall method of braking before impacting the trunk of a tree (Bahlman et al., 2012; Khandelwal and Hedrick, 2020). Birds can manage a stall method as well, however, many birds use slow, flapping flight during landing instead, despite it being energetically costly (Usherwood, 2005). Therefore, it appears that perching birds landing on a solid substrate use their ability to generate additional aerodynamic forces through powered flight to increase deceleration just before impact. If so, then the mallards are braking less than either of these groups, yet they also use powered flight to brake before impact. This difference in degree of braking between perching birds and mallards is most likely due to the change in the compliance of the substrate. Goats maintain balance under conditions in which the compliance of the substrate is different by modulating the stiffness of their hindlimbs (Clites et al., 2019). This is a fairly slight adjustment and mallards may be doing the same thing. Instead of developing a unique way to regulate how to land on water, they are retaining the same regulatory strategy and corresponding behavior as perching birds except they brake less. This likely saves energy and allows the more compliant water surface to absorb the kinetic energy that could be injurious on a more rigid substrate.

In addition, pigeons during perch landing have been recorded at velocities consistently below 2 m/s (Berg and Biewener, 2010; Green and Cheng, 1998), while mallards do land within this lower range, they will also land at velocities up to 8.5 m/s, over a 4x increase in impact

speed. Approach angle in the ducks (8.6° ± 6.3°) appears to largely coincide with perhaps slightly more horizontal trajectories, compared to pigeons where the typical mean trajectory angle is between 10° to 15° (Green and Cheng, 1998). However, mallards appear to typically impact at a shallower angle. Pigeons were found to contact a perch at an 80° to a 50° angle (Green and Cheng, 1998), whereas mallards impacted the water at a mean angle of 14.8 ± 10.0 degrees, with an upper limit of 59.9°. Together, the data on $\dot{\tau}$ and the kinematics suggest that while mallards water landing behavior is visually regulated in the same fashion as other flyers, mallards often decelerate less and impact at much greater velocities.

2.5 *Conclusions*

Mallards landing on water utilize a similar $\dot{\tau}$ constant braking strategy as that which has been documented in the landing behavior of pigeons and bats, as well as during feeder approach in hummingbirds. Yet, the $\dot{\tau}$ values used by the ducks are much higher suggesting less deceleration even if they are braking using the same strategy. In addition, impact speeds are as much as 4x higher than seen in pigeon perch landing behavior. These two differences observed in landing behavior compared to pigeons perching implies that mallards may be taking advantage of the inertial absorptive properties of landing on water to disperse higher velocity landings with less deceleration. However, this study does not discern whether the differences in landing behavior between mallards and pigeons is an active behavioral shift or passive affect due to how optic flow is perceived. The change in kinematics and $\ddot{\tau}$ values could be active as a way to preserve energy expenditure during landing or be a side effect of a decreased ability to

discern τ while landing on a more featureless water substrate, which could lower the accuracy of their perception of optic flow.

2.6 *References*

Altshuler, D. L. and Srinivasan, M. V. (2018). Comparison of visually guided flight in insects and birds. *Front. Neurosci.* **12**,.

Bahlman, J. W., Swartz, S. M., Riskin, D. K. and Breuer, K. S. (2012). Glide performance and aerodynamics of non-equilibrium glides in northern flying squirrels (Glaucomys sabrinus). *J. R. Soc. Interface* **10**, 20120794–20120794.

Baird, E., Boeddeker, N., Ibbotson, M. R. and Srinivasan, M. V. (2013). A universal strategy for visually guided landing. *Proc. Natl. Acad. Sci.* **110**, 18686–18691.

Berg, A. M. and Biewener, A. a (2010). Wing and body kinematics of takeoff and landing flight in the pigeon (*Columba livia*). *J. Exp. Biol.* **213**, 1651–8.

Bhagavatula, P. S., Claudianos, C., Ibbotson, M. R. and Srinivasan, M. V. (2011). Optic flow cues guide flight in birds. *Curr. Biol.* **21**, 1794–1799.

Chakravarthi, A., Rajus, S., Kelber, A., Dacke, M. and Baird, E. (2018). Differences in spatial resolution and contrast sensitivity of flight control in the honeybees *Apis cerana* and *Apis mellifera*. *J. Exp. Biol.* **221**, jeb184267.

Clites, T. R., Arnold, A. S., Singh, N. M., Kline, E., Chen, H., Tugman, C., Billadeau, B., Biewener, A. A. and Herr, H. M. (2019). Goats decrease hindlimb stiffness when walking over compliant surfaces. *J. Exp. Biol.* **222**, jeb198325.

Dakin, R., Fellows, T. K. and Altshuler, D. L. (2016). Visual guidance of forward flight in hummingbirds reveals control based on image features instead of pattern velocity. *Proc. Natl. Acad. Sci.* **113**, 8849–8854.

Gibson, J. (1958). Visually controlled locomotion and visual orientation in animals. *Br. J. Psychol.* **49**, 182–194.

Green, P. and Cheng, P. (1998). Variation in kinematics and dynamics of the landing flights of pigeons on a novel perch. *J. Exp. Biol.* **201**, 3309–3316.

Hart, V., Malkemper, E. P., Kušta, T., Begall, S., Nováková, P., Hanzal, V., Pleskač, L., Ježek, M., Policht, R., Husinec, V., et al. (2013). Directional compass preference for landing in water birds. *Front. Zool.* **10**, 1–10.

Jackson, B. E., Evangelista, D. J., Ray, D. D. and Hedrick, T. L. (2016). 3D for the people: multi-camera motion capture in the field with consumer-grade cameras and open source software. *Biol. Open* **5**, 1334–1342.

Johnsgard, P. A. (2010). Tribe Anatini (Surface-Feeding Ducks). In *Ducks, Geese, and Swans of the World* (ed. Nebraska, U. of), pp. 216–219. Lincoln.

Khandelwal, P. C. and Hedrick, T. L. (2020). How biomechanics, path planning and sensing enable gliding flight in a natural environment. *Proceedings. Biol. Sci.* **287**, 20192888.

Koenderink, J. J. (1986). Optic flow. *Vision Res.* **26,** 161–180.

Lee, D. N. (1976). A theory of visual control of braking based on information about time-to-collision. *Perception* **5**, 437–459.

Lee, D. N., Reddish, P. E. and Rand, D. T. (1991). Aerial docking by hummingbirds. *Naturwissenschaften* **78**, 526–527.

Lee, D. N., Davies, M. N. O., Green, P. R. and Van Der Weel, F. R. (1993). Visual control of velocity of approach by pigeons when landing. *J. Exp. Biol.* **180**, 82–104.

Lee, D. N., Simmons, J. A., Saillant, P. A. and Bouffard, F. (1995). Steering by echolocation: a paradigm of ecological acoustics. *J. Comp. Physiol. A* **176**, 347–354.

Lee, D. D. N., Bootsma, R. J., Land, M., Regan, D. and Gray, R. (2009). Lee's 1976 paper. *Perception* **38**, 837–858.

Linander, N., Dacke, M. and Baird, E. (2015). Bumblebees measure optic flow for position and speed control flexibly within the frontal visual field. *J. Exp. Biol.* **218**, 1051–1059.

McMahon, T. A. (1985). The role of compliance in mammalian running gaits. *J. Exp. Biol.* **115**, 263–282.

Scaramuzza, D., Martinelli, A. and Siegwart, R. (2006). A toolbox for easily calibrating omnidirectional cameras. *IEEE Int. Conf. Intell. Robot. Syst.* 5695–5701.

Srinivasan, M. V, Zhang, S. W., Lehrer, M. and Collett, T. S. (1996). Honeybee navigation *en route* to the goal: Visual flight control and odometry. *J. Exp. Biol.* **199**, 237–244.

Taylor, G. K. and Krapp, H. G. (2007). Sensory systems and flight stability: what do insects measure and why? *Adv. Ins. Physiol.* **34,** 231-316.

The Meteorological Glossary (1961). 3rd ed. London: Her Majesty's Stationery Office.

Usherwood, J. R. (2005). Dynamic pressure maps for wings and tails of pigeons in slow, flapping flight, and their energetic implications. *J. Exp. Biol.* **208**, 355–369.

Vo, H. D., Schiffner, I. and Srinivasan, M. V. (2016). Anticipatory manoeuvres in bird flight. *Sci. Rep.* **6**, 1–8.

Wang, H., Ando, N., Takahashi, H. and Kanzaki, R. (2017). Visuomotor response to object expansion in free-flying bumble bees. *J. Insect Behav.* 1–20.

Yu, B., Gabriel, D., Noble, L. and An, K. N. (1999). Estimate of the optimum cutoff frequency for the Butterworth low-pass digital filter. *J. Appl. Biomech.* **15**, 318–329.

Zhang, Z. (2000). A flexible new technique for camera calibration. *IEEE Trans. Pattern Anal. Mach. Intell.* **22**, 1330–1334.

Chapter 3

Mallard landing approach kinematics driven primarily by horizontal impact velocity

Abstract

The kinematics of flight is a great source of bioinspired and biomimetic design, however most studies of flight are restricted to the laboratory due to the methodological constraints of collecting accurate kinematic measurements through photogrammetry. Recently, methods have been developed that allow some of these methods for tracking movement in 3D to be taken into the field, which has stimulated research on flight behaviors that are difficult to replicate within a laboratory setting. One such behavior is landing on water, for which the logistics of creating a body of water large enough to allow ducks to land on naturally has been prohibitive. Therefore, in this study the landing behavior of mallards was filmed in the natural environment through the use of two separate camera systems. The first was focused broadly and allowed for single point tracking of the ducks to obtain landing trajectory position in space. From the digitized trajectories vertical impact velocity, horizontal impact velocity, impact angle, mean approach angle, and distance after impact could be calculated. The second allowed for a closer view of the bird at impact and its transition into the water. From the digitized points on the mallard the relative movement of the parts of the duck could be tracked for the duration of the transition from the initial impact with the water until the breast impacted the surface. Through the combination of these two camera systems 177 landing trajectories were recorded; of those 24 also had footage of the transition into the water. From this dataset general linear models suggest that the only approach and transition kinematic parameters that have significant influence on distance after impact are horizontal impact velocity, impact angle, and mean approach angle. Of those three, horizontal impact velocity accounts for the majority of variation explained by this model, 22% out of 26%. A principle component analysis (PCA) based on the three primary kinematics found by the general linear model was also done. The PCA, combined with a k-clustering algorithm implies that there are two different kinematic profiles documented in this study. The first, a typical landing (N=119), tends to have higher velocities, shallower approaches, and shallower impact angles. Besides being the majority of landings in the dataset the kinematic profiles for these landing are more consistent with each other. The second, an atypical landing (N=58), tends to have slower velocities, steeper approaches, and steeper impact angles. These landings tend to have much more variable kinematic profiles. The results demonstrate that the primary kinematic associated with shifts in landing kinematics is horizontal impact velocity. In addition, mallards appear to have a tendency to land on water with shallow high speed landings, but do occasionally land at steeper slower speeds.

3.1 *Introduction*

The kinematics of flight has been a frequent source of biomimetic research and as a result there is a large breadth of work looking at the morphology and, more recently, the kinematics of how birds and other flyers generate lift to inform our own aeronautical constructions. However, despite this long history of biomimetic design from the avian wing leading to our airplanes' airfoils up to the modern efforts to make drones with actively flapping wings, there is a surprising lack of focus on the interfaces of flight locomotion - takeoff and landing. Particularly with regard to landing on water, the kinematics have only been examined once (Norberg and Norberg, 1971). This study examined the landing behavior of the red-throated loons (*Gavia stellata*) which land breast first, as opposed to feet first (Norberg and Norberg, 1971). To capture quantitative aspects of takeoff velocity was derived from sequences of still images taken at five frames per second and one takeoff was recorded on video at 200 fps (Norberg and Norberg, 1971). From these images and video ground speed was calculated to be 10 m/s for complete liftoff, after a transitionary locomotive mode where the loons skitter along the surface of the water for 15-40 m (Norberg and Norberg, 1971). Landings, unlike takeoff, for these birds frequently include a bank and so the same method for estimating velocity and distance traveled from one perspective for the linear takeoff behavior could not be applied to landing (Norberg and Norberg, 1971). However, today photogrammetric techniques have seen huge advances leading to a significant increase in the spatial and temporal quality of footage that can be obtained as well as the accuracy with which we can calculate quantitative measures of movement based on those images.

As a result of these technological and methodological advances, studies employing photogrammetric techniques in the laboratory have been conducted to examine the kinematics of flight in insects (Fry et al., 2005; Hedrick and Daniel, 2006; Ristroph et al., 2013), bats (Bergou et al., 2015; Wolf et al., 2010), and birds (Ros et al., 2011; Tobalske et al., 2007; Wolf et al., 2013). Research is now also ongoing into implementing the differences in analogous forms of flight, such as hovering or slow flight, across such disparate taxa to inform aerial robotics (Vejdani et al., 2019). However, due to the logistical challenges of observing a behavior in multiple cameras from multiple points of view, most of these studies have examined flight under controlled laboratory conditions in which the subject flies from one perch to another, hovers in place, or is artificially held in place with a wind tunnel – in all the behavior is inherently constrained to a limited volume. The inherent restrictions of these methods limit our ability to understand the diverse number of flight behaviors performed by flyers. To enable us to quantify a broader variety of flight behavior tools to employ photogrammetric techniques effectively in the field are becoming more common (de Margerie et al., 2015; Ling et al., 2018; Theriault et al., 2014). Using these newer techniques, scientists have begun to examine the flight kinematics of these large-scale flight maneuvers such as group flight behavior in chimney swifts (Evangelista et al., 2017), searching behavior in the common swift (de Margerie et al., 2018), and gliding in *Draco* lizards (Khandelwal and Hedrick, 2020).

Landing on water is difficult to replicate in a laboratory setting due to the difficulty of creating a lab space with enough space to house a body of water that ducks can fly to, land in, and still skim. Ducks do not always stop on impact in water, but can and do travel up to several meters after impact. In this study several methods are employed to enable us to take

photogrammetric techniques into the field to more closely examine the kinematics of how mallards land on water.

Chapter 2 used kinematic data to demonstrate that mallards regulate landings using the same $\dot{\tau}$ constant braking strategy as seen in perch landings in pigeons (Lee et al., 1993). However, the data also showed that the range of approach kinematics at which mallards land on water is much broader than what has been seen for pigeons landing on a perch**.** In fact, several studies demonstrate that pigeon landings (Berg and Biewener, 2010; Green and Cheng, 1998; Lee et al., 1993) have maximum impact speeds around 2 m/s and relatively steep impact angles between 50° to 80° (Green and Cheng, 1998). Mallards land at impact speeds up to 4x greater and have a mean impact angle 3x shallower than the lower end of impact angles documented in pigeons. If we consider the momentum these kinematics suggest pigeons and mallards have on impact the difference is even greater. Based on the mean masses reported in previous kinematic studies of pigeons the approximate average mass for an individual is 460 g ± 30 g (Berg and Biewener, 2010; Green and Cheng, 1998; Ros et al., 2011) while mallards are approximately 1,000 g (Johnsgard, 2010) resulting in the greatest potential momentum at impact for each bird being 0.83 kg·m/s and 8.35 kg·m/s respectively. This implies the maximum momentum with which a mallard impacts the water is an order of magnitude above the maximum momentum at which a pigeon impacts a perch. However, despite the differences both the distributions of impact speeds and impact angles observed in mallards overlap with the comparatively more constrained ranges seen in perch landings in pigeons. Here, we examine the kinematics of approach, transition, and result of mallards landing behavior to better understand what kinematics are primary drivers of the behavior.

3.2 *Methods*

To examine the kinematics of landing in mallards the same digitized landing trajectories which were collected in Chapter 2.2 were used. These landing flights were recorded at a local pond on 3 videocameras (HERO4 Black, GoPro, Los Angeles, CA, USA) placed along a section of shoreline. The cameras recorded at a resolution of 4k and 30 fps, were synced post-hoc based on sound pulses, de-warped based on omnidirectional distortion coefficients (Jackson et al., 2016; Urban et al., 2015), and calibrated through the use of 0.94 m wand (Jackson et al., 2016; Zhang, 2000). The maximum digitization error on a given calibration for the dataset is ±2.18 cm. See Chapter 2.2 for further details.

However, an additional camera tracking setup was constructed to be used in tandem with the 3 GoPro camera array described above. This second tracking setup is derived from the work of Margerie et al. (2015) and it enables its user to zoom into and track the subject from a distance while viewing its movements from two slightly different perspectives simultaneously. These two perspectives enable photogrammetric techniques to measure the physical movements of an organism close up while still in the field (de Margerie et al., 2015). This new camera system, termed a Rotational Stereo Videography (RSV) rig, is constructed from a rigid T-shaped frame (de Margerie et al., 2015). The cross on top is approximately a meter long with angled reflected mirrors on either end with two mirrors in the middle of the cross angled to reflect the image observed by the ends back towards the base of the T. At the base of the T is placed a DSLR, upon which the lens can be placed, which receives the two images reflected back towards it simultaneously. This array of mirrors creates a split image viewed by the

camera, in which each half of the image can then be treated as a separate camera view and photogrammetric techniques, such as DLT, can be used to calculate the position of objects by comparing the two perspectives (de Margerie et al., 2015).

For this study, the RSV rig described cannot give global position as the rig pans horizontally on the tripod. However, it can still accurately give relative measurements to a point within the frame, which is the purpose for which we implemented this second RSV rig. The data collected from the GoPro Array (details in Ch. 2.2) allows tracking of global kinematic position of the duck during approach and through impact, thereby enabling the determination of position in 3D and the calculation of velocities and angles associated with the variety of landings observed. This RSV rig enabled us to examine the changes in posture of a subset of these ducks at the point of impact and track how the head and body move in relation to each other through the transition from flight to skimming on the surface of the water.

The rig was constructed of 80/20 aluminum (80/20 Inc., Columbia City, IN, USA), with a T-cross spanning 1 m and two beams extending backwards 1 meter back. The beams extending back have cross-beams half way and at the end far from the cross. These cross-beams provided extra support, and also served as points of attachment for the rig to the tripod and camera. In addition, angled support struts from the parallel beams to the cross were included to prevent oscillations due to bending of the cross bar, which occurred under low wind conditions when the mirrors were attached. Four first-surface mirrors (First Surface Mirror LLC, Toledo, OH, USA) were used to create the mirror array**.** The two mirrors on the ends were 300 x 150 mm and the center pair were 150 x 150 mm and each had a 45° miter cut ground onto one side. The mirrors were glued, reflective side facing out, to 0.3125” aluminum plates of matching size (Midwest

Steel Supply Inc., Rogers, MN, USA) in which two holes were drilled to allow for the attachment of two right-angle ¼”post clamps (Thorlabs Inc., Newtown , NJ, USA) to the back of each mirror. The mirrors were then attached to the RSV frame by slipping the post clamps over 3” tall optical posts (TR3-P5, Thorlabs Inc., Newtown, NJ, USA) to secure them in place. The posts for the mirrors on the end were secured into 2” rotational stages (Thorlabs Inc., Newtown, NJ, USA) to enable manual rotation of each and for the angles to be matched. The posts for the center mirrors were attached to a single-axis translational stage (PT1, Thorlabs Inc., Newtown, NJ, USA), with the 45° miter cut edges flush against each other to create 90° reflective corner with the least amount of lost image reflecting into the camera. By placing the mirrors on these rotational and translational stages the RSV could be assembled with precision to the same arrangement for each filming session. This system enabled continuity between filming sessions. The camera used to record the landing data was a Nikon DSLR 800 (Nikon Inc., Melville NY, USA) which recorded at 1920 x 1080p 120fps with a 105 mm fixed focal length lens for subjects that were impacting approximately 20 meters from the camera. All of this: T-frame, mirrors, and camera were mounted upon a tripod

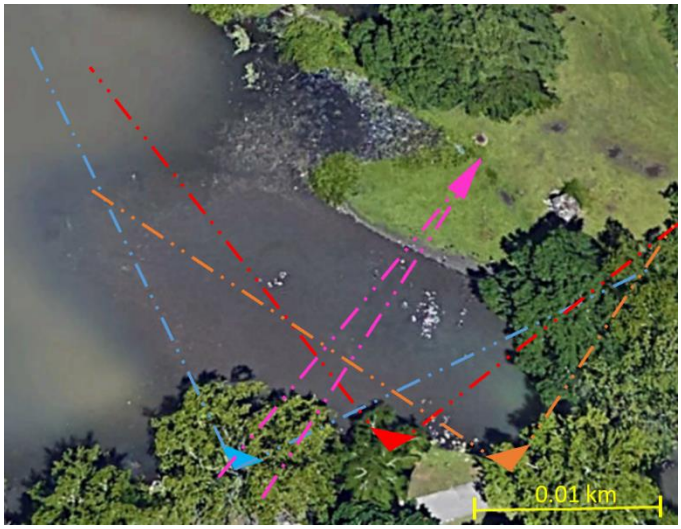

Figure 3.1: Shows the pond at which filming occurred including the GoPro positions and approximate view in blue, red, and orange. The position and view of the RSV is shown in pink. Note the view of the RSV can and does pan horizontally to track to individuals, but the view shown is representation of what the camera can at one point in time.

with a fluid head (Manfrotto 545B tripod and 509 HD head, Vitec Imaging Distribution Inc., Saddle River, NJ, USA).

The rig was set up on the opposite shore from the GoPro array (Fig. 3.1). This placement was employed in part to improve tracking of the mallards with the RSV, as this shore provides the viewer with a greater ability to see mallards approach the filming cove. Two people are required to run both the RSV rig and GoPro array together. One person operates the RSV, tracking and recording any mallards who land in the vicinity. Meanwhile, the other individual triggers the GoPro's remotely when mallards approach the area of interest. The individual responsible for the GoPro array would also distribute the cracked corn used to feed the ducks, as described previously in Chapter 2.2.

Camera intrinsic parameters for the DSLR 800 were found using Argus Patterns features and all video was de-warped based on those intrinsic parameters (Jackson et al., 2016). Using these parameters a zone in front of the RSV was calibrated using a 0.29 m long wand, using the same methods as outlined in Chapter 2.2. The maximum variance seen in wand length for a given digitization was ±1.3 cm.

Videos from the RSV were matched to corresponding GoPro videos based on timestamps and visual identification based on proximity to other birds in the video. In total there were 45 videos identified in which the landing was recorded by both the GoPro's and RSV camera arrays; of those 24 could be reliably digitized. For each RSV sequence the shoulder and base of tail were digitized through the transition into the water. Gaps in the digitization from frames where a digitized part of the body could not be seen were interpolated using a cubic

spline. Then, a consistent frame of reference of all the points was fixed relative to the position of the mallard's shoulder. The position of the shoulder was subtracted from all points in the dataset for each corresponding point in time to make the shoulder of the duck the origin for all further processing. The resulting position data for each point was filtered using a 2^{nd} order Butterworth filter (Yu et al., 1999).

Lastly, the position data of the points was used to calculate the range of motion of the body. All angles are calculated relative to the horizontal. In practice, horizontal was found by creating a hypothetical point at the same height of the xy-plane of the vertex point of the angle and was positioned laterally below the end point of the ray extending to a known point on the subject's body. Body angle was calculated with the base of the tail as the vertex and shoulder as the ray; the head angle was calculated with the shoulder as the vertex and the base of bill as the ray; and gaze angle was calculated with the base of the bill as the vertex and the tip of the bill as the ray. Transition duration is defined as the time from initial impact until the breast impacts the water surface.

From the GoPro camera array, vertical impact velocity, horizontal impact velocity, impact angle, mean approach angle, and distance after impact were calculated as described in Chapter 2.2. The definitions for each kinematic parameter are shown again in Table 3.1.

To analyze the data, regression analyses were run on all approach kinematics with relation to the resulting kinematic parameter, distance after impact. In addition, a general linear model (GLM) was run on the approach kinematics in relation to the distance after impact. The GLM was based on the gamma distribution of the resultant variable, distance after impact, and due to the exponential and logarithmic nature of the relationships between distance after impact and horizontal impact velocity, impact angle, and mean approach all data was log transformed for GLM.

In addition, regression analyses were run on the subset of the larger dataset, 24 landings, in which the landing trajectory could be tracked by the GoPro array and by the RSV rig. This was done for all the previously mentioned approach kinematics and the transition kinematics of transition duration and body angle with respect to distance after impact. A second general linear model was also run on this subset of data, retaining the same parameters as the previous.

Table 3.1: All kinematic parameters collected from digitization data in both the GoPro camera array and from the RSV rig. Vertical impact velocity, horizontal impact velocity, impact angle, and mean approach angle are all collected from digitized landing trajectories from the GoPro array and considered to be approach kinematics. Distance after impact is also collected from digitized landing trajectories from the GoPro array, but is considered a resultant kinematic. Transition duration and range of motion of the body are collected from digitization of the landings from the RSV rig and are considered to be transition kinematics.

Kinematic	Definition
Vertical impact velocity	Vertical velocity in the z-axis at the moment of initial impact
Horizontal impact velocity	Horizontal velocity in the x-axis at the moment of the initial impact
Impact angle	Angle of velocity vector at the moment of initial impact
Mean approach angle	Mean of all velocity vector angles for the approach up till the moment of impact
Distance after impact	Distance traveled after initial impact
Transition duration	The duration from initial impact with the water until the breast impacts the water
Range of motion of the body	Angle a line from the shoulder to base of tail makes with the water at initial impact

A principle component analysis (PCA) was run on the larger dataset (n=177) which included the parameters suggested by the GLM to have the most influence on distance after impact: horizontal impact velocity, impact angle, and approach angle. A K-cluster algorithm was employed to examine the possibility that distinct behaviors may account for some of the variation seen in the landing data. The dataset was then split based on the results of the K-cluster algorithm and regression analyses with respect to distance after impact were re-run based on those suggested groupings.

3.3 *Results*

Table 3.2: The mean, standard deviation, and range are shown for all kinematic parameters collected from the GoPro array (N = 177) and RSV rig (N=24). Vertical impact velocity, horizontal impact velocity, impact angle, mean approach angle, and distance after impact are all based on a larger dataset of landing collected from the GoPro recordings. Transition duration and range of motion of the body are based on data collected from a smaller dataset in which the landings were viewed in both the GoPro and RSV camera systems.

Kinematic	Mean	SD	Range
Vertical impact velocity	-1.09 m/s	±0.45 m/s	-3.05 m/s, -0.08 m/s
Horizontal impact velocity	4.84 m/s	±1.48 m/s	0.88 m/s, 8.35 m/s
Impact angle	14.8°	±10°	0.6°, 59.9°
Mean approach angle	8.6°	±6.3°	-0.4°, 36.7°
Distance after impact	2.17 m	±1.36 m	0 m, 6.04 m
Transition duration	125 ms	±62 ms	50 ms, 266 ms
Range of motion of the body	33°	±20°	5°, 76°

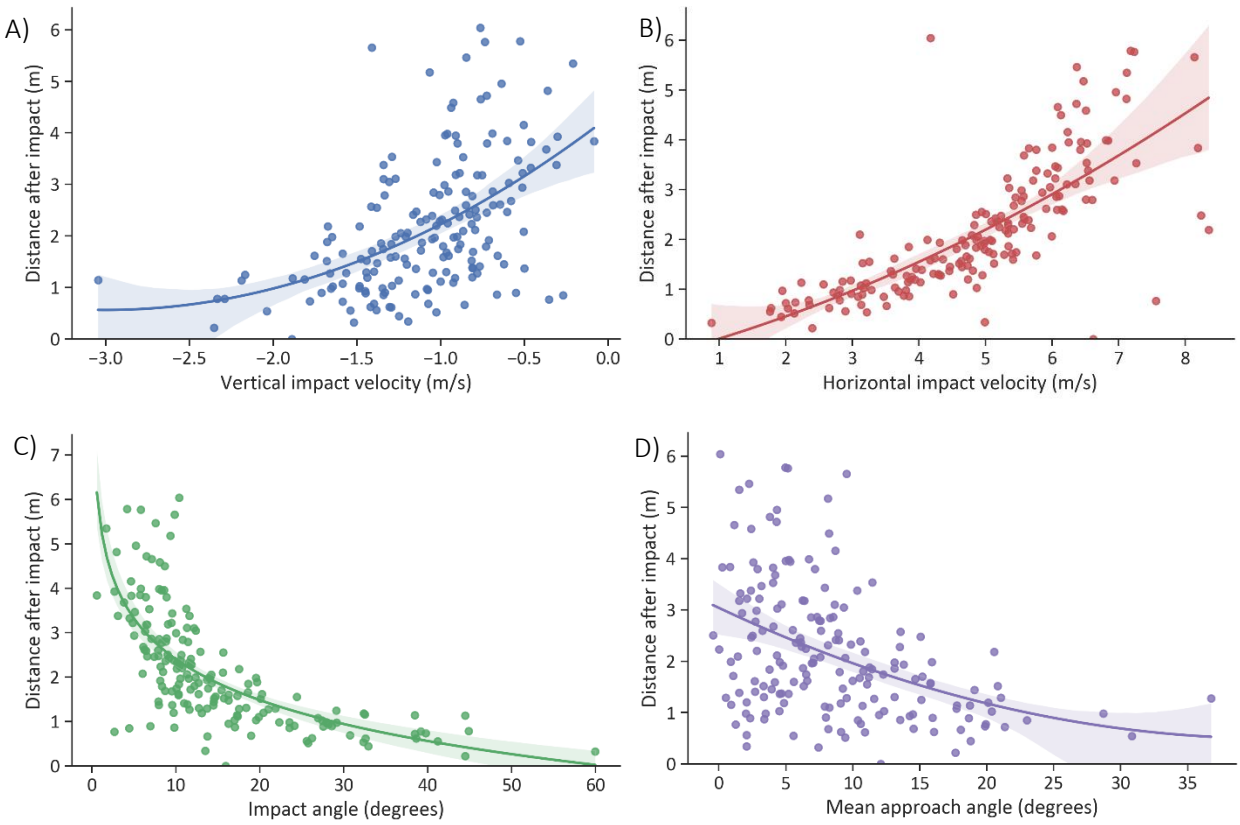

Figure 3.2: Regression analysis of the approach kinematics with respect to distance after impact (N=177). Vertical impact velocity ($p < 0.01$) shown in blue (A), horizontal impact velocity ($p < 0.01$) shown in red (B), impact angle ($p < 0.01$) shown in green (C), and mean approach angle ($p < 0.01$) shown in purple (D). The shaded region is a bootstrapped standard error of the data to the line of best fit.

The mean, standard deviation, and range are shown in Table 3.2 for all kinematic parameters obtained from landings recorded on the GoPro camera array (N=177). From these results, regressions were performed for each approach kinematic with respect to distance after impact, revealing that all four approach kinematics have significant relationships to distance after impact. Vertical impact velocity has a positive trendline, however there is dramatic shift in the range and variation of distances after impact for descent rates above -1.5 m/s as opposed to a tightly correlated exponential relationship below -1.5 m/s. Horizontal impact velocity also has a positive trend with respect to distance after impact. However, the exponential relationship appears to hinge around a shift in the relationship of the two parameters around the horizontal

impact velocity of 5 m/s. Impact angle has a strong logarithmic negative relationship to distance after impact. It would appear that once the impact angle is higher than 20° mallards do not skim further than 2 m after impact. Mean approach angle also has a negative relationship to distance after impact. Steeper approach angles appear to lower skim distance, while shallower approaches have little effect on a mallard's ability to make a short skim after impact.

Table 3.3: Results of a GLM (family: gamma, link: logarithmic) comparing all approach kinematic to distance after impact (N=177).

Parameter	Coefficient	Standard Error	P-value
Mean approach angle	-0.02	0.005	0.001
Impact angle	-0.02	0.005	0.000
Horizontal impact velocity	0.22	0.011	0.000
Vertical impact velocity	-0.01	0.109	0.936

A general linear model (GLM) was used to determine how the various approach kinematics measured may influence the distance after skimmed (Table 3.3). The GLM revealed that despite the relationships shown by the regression analyses, vertical impact velocity is not a significant contributor to distance after impact. In addition, mean approach angle, impact angle, and horizontal impact velocity are significant contributors. Of those three, horizontal impact velocity has the highest coefficient, 0.22, suggesting it is the primary

Table 3.4: Results of a GLM (family: gamma, link: logarithmic) comparing approach kinematics and transition time to distance after impact (N=24).

Parameter	Coefficient	Standard Error	P-value
Mean approach angle	-0.002	0.009	0.807
Impact angle	-0.025	0.015	0.085
Horizontal impact velocity	0.203	0.036	0.000
Vertical impact velocity	-0.028	0.280	0.921
Transition time	0.001	0.001	0.405

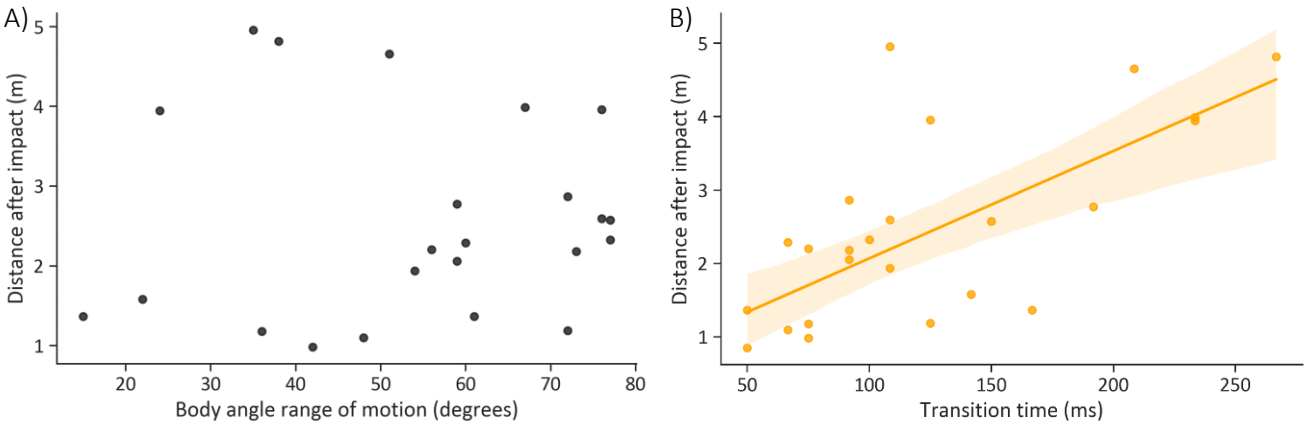

Figure 3.3: Regression analyses of transition kinematic parameters with respect to distance after impact. The scatter plot in black (A) shows the lack of a clear relationship between the ranges of motion covered by body of each duck while transitioning their breast into the water with respect to distance after impact (N=23). In yellow (B) is the positive relationship present between the duration, in milliseconds, it takes for each duck to transition into the water after initial impact and distance traveled after impact (N=24).

driver of distance after impact. In comparison, mean approach angle and impact angle each account for 0.02 of the variation observed in distance after impact. However, this means that cumulatively horizontal impact velocity, impact angle, and approach angle account for merely 26% of the variation observed in distance after impact.

For landings that were recorded on both the GoPro array and RSV rig (N = 24), regressions were applied for body angle range of motion and transition duration with respect to distance after impact. Of these two transition kinematics, only transition duration has a statistically significant relationship ($p < 0.01$), while the range of motion of the body angle has no influence on distance after impact. The GLM on this subset of data (N=24), for all previous approach kinematics with transition time included (Table 3.4), implies that the sole significant contributor to distance traveled after impact is horizontal velocity. However, the coefficient for horizontal impact velocity is 0.203 in this analysis. Therefore, the current parameters explain only a fraction of the variation in distance after impact.

Based on the results of both GLMs, the only parameters that are likely significant contributors to distance after impact are horizontal impact velocity, impact angle, and mean approach angle. However, these parameter are not completely independent of each other, therefore a three dimensional principle component analysis (PCA) was done based upon those three kinematic parameters to see how these parameters may combine to create distinct kinematic profiles based on horizontal impact velocity, impact angle, and mean approach angle. Once the principle components were plotted a K-cluster algorithm was employed to detect and highlight any clusters of consistent kinematic profiles present in the data (Figure 3.4). The

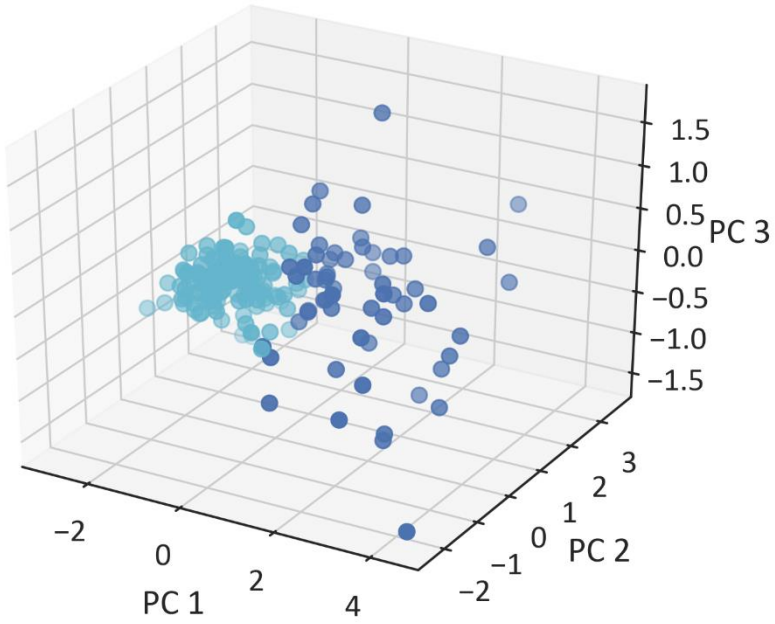

Figure 3.4: Principle component analysis (PCA) in which the three approach kinematics were used: horizontal impact speed, impact angle, and mean approach angle. These approach kinematics are the three which are suggested to be significant contributors by the GLM (N=177) to the resulting kinematic parameter, distance after impact. The results of the PCA are colored based on a K-cluster analysis, which suggests there may be two distinct approach kinematic behaviors within the dataset. The first shown in dark blue appears to be characterized by less variation along each principle component, while the second behavior is positive along the 1st principle component with increased variation in both directions along both the 2nd and 3rd principle components.

resulting PCA with K-cluster algorithm suggests that there are no strong delineations or disparate clustering based on these kinematic parameters. However, there is a potential split in the dataset primarily along the 1st principle component. Based on this clustering greater values along PC 1 are consistently linked to increased variation along the other two principle components. Based on this clustering the approach kinematics were readdressed with respect distance after impact with these two groups separated. For the purposes of further analysis the landings with less variation and that occur in greater numbers in the dataset (N=119) are considered to be typical landings. Therefore, the other landings with more variable kinematics (N=58) are considered to be atypical landings. These two groups, typical and atypical, were used to reexamine the

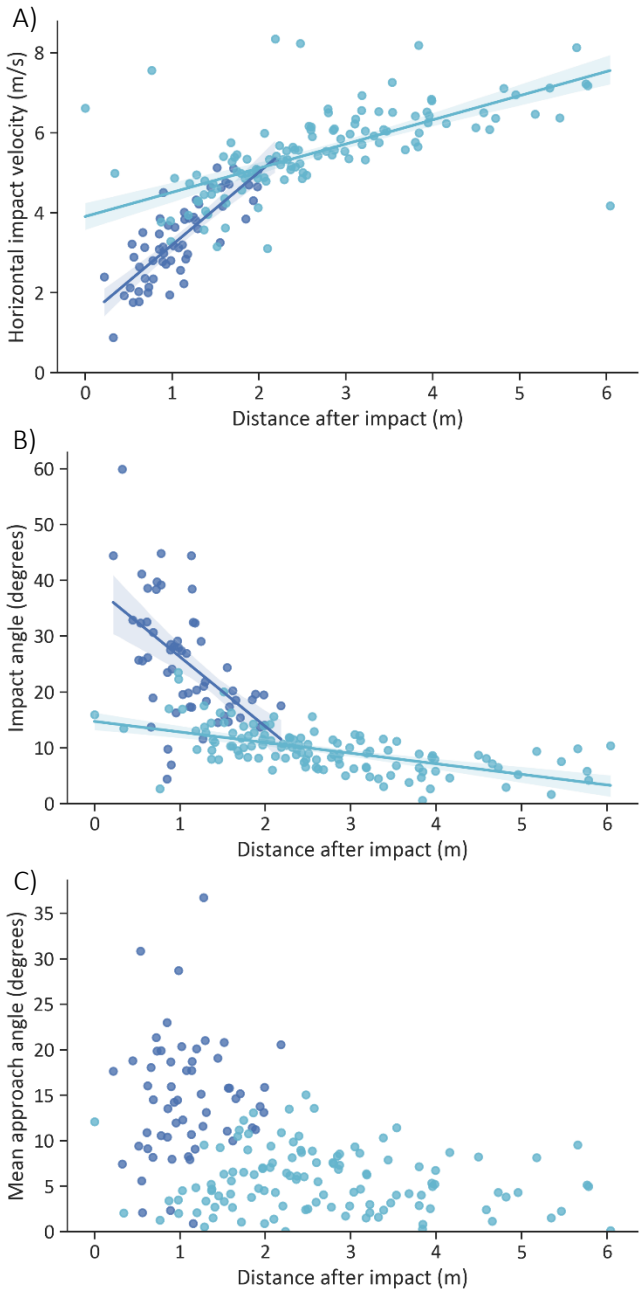

Figure 3.5: Regression analyses of approach kinematics to distance after impact for both atypical landings (N=58) shown in dark blue and typical landings (N=119) shown in light blue. Horizontal impact velocity (A) and impact angle (B) both retain statistically significant relationships ($p < 0.01$) to distance after impact for both typical and atypical landings. However, the mean approach angle (C) does not for either group ($p > 0.05$).

relationships between the key approach kinematics horizontal impact velocity, impact angle, and mean approach angle to the resultant kinematic, distance after impact. When grouped based on the clustering from the PCA, both horizontal impact velocity (Pearson linear regression, $p < 0.01$) and impact angle (Pearson linear regression, $p < 0.01$) retain significant trends with relation to distance after impact for both typical and atypical landings. Mean approach angle does not have a significant relation to distance after impact (Pearson linear regression, $p > 0.05$). However, the groups are clearly distinct for each kinematic parameter and imply these atypical landings, in comparison to typical ones, frequently have higher mean approach angles, higher impact angles, and slower horizontal impact velocities. In addition, for impact angle and horizontal impact speed the slopes of the relationship each category of landing has to distance after impact are distinct. The typical landing behavior has a slope of -1.9 with regard impact angle, while atypical landings have a slope of -12.7. With regards to horizontal impact velocity typical landings have a slope 0.5, while atypical landings have a slope of 1.8. These increased slopes in the negative and positive directions are representative the greater variation seen in atypical landings compared to a typical landing. These differences also lead to atypical landings not traveling as far after impact. The mean distance traveled after impact for atypical landings which is 1.09 ± 0.46 m, while typical landings have a mean and standard deviation of 2.68 ± 1.24 m.

3.4 *Discussion*

This study has focused on a specific feature of landing on water, distance after impact, and examined what kinematic parameters of the landing approach and transition into the water

may contribute most to the distance traveled after impact. The results of general linear models, including approach and transition kinematics, implicate horizontal impact velocity as the primary driver of how far a mallard will travel after impacting the water. Other relevant parameters were found to be impact angle and mean approach angle, but the coefficients in the model suggest the contribution to distance after impact is minimal in comparison to that of horizontal impact velocity. This result is intuitive, as it suggests that the velocity of a mallard in the horizontal direction when it impacts the water surface is highly predictive of how far it will travel horizontally across the surface of the water. Secondarily, the angle of impact with the water surface and how steep or shallow an individual's approach trajectory does affect the result, but large changes in those angles are needed to see a slight change in the distance traveled after impact. What is more surprising is what does not significantly influence the distance a mallard travels after landing which are: vertical impact velocity, transition time, and the arc angle the body covers as it lowers into the water. That is not to say that these physical aspects of landing, how quickly a bird is descending, how long it takes to lower their breast into the water, and the range of motion of the breast while transitioning into the water cannot influence the distance after impact. Instead, the range of kinematics at which mallards land for each of these parameters are largely irrelevant to the end result of the landing.

Of those parameters that are relevant to distance after impact, horizontal impact velocity, impact angle, and mean approach angle, all have low coefficients. As a result, less than 25% of the variation documented in distance after impact is accounted for in these models. Therefore, additional variables likely contribute to distance after impact which are not accounted for in this study. Based on qualitative assessments of the landings some likely

candidate variables are the following. First, some ducks visibly lunge into the skim at the end of the transition phase, shifting their center of mass during the transition phase and while skimming. Second, regulating the shape of the breast and feet while in contact with the water during the transition and skim could adjust the main drag and lift surfaces for water flow, thereby influencing the distance traveled after impact. Last, the ducks may add additional thrust by paddling with their feet during a skim.

Besides exploring the potential importance of individual kinematic parameters to landing in mallards, this work was done in the field. Therefore, there is the possibility that some of the variation seen in the kinematics are due to shifts in landing behavior from external factors, such as obstacles in the landing area. The principle component analysis done using the key approach kinematics (Figure 3.4) showed no distinct groupings suggestive of dramatic shifts in those kinematics. However, a K-cluster algorithm does suggest there are potentially two broad, continuously distributed groups. The typical landings (N=119) are comparatively consistent, forming a tight cluster with regards to kinematic profile. The other, atypical landings (N=58), are shifted consistently with respect to PC1 from typical landings and have non-directional increases in variation with regard PC2 and PC3 (Figure 3.4). Closer examination at how the individual approach kinematics make up these kinematic profiles with regards to distance after impact (Figure 3.5) gives a clearer picture of what may be the cause of these shifts in kinematics. Typical landings have comparatively high horizontal impact speeds with shallow impact angles and shallow approach trajectories commonly resulting in longer skims after impact. Meanwhile, atypical landings have lower horizontal impact velocities with higher impact angles and steeper approach trajectories which tend toward less skimming after impact.

The kinematic factors of these two groups suggests that atypical landing may be a behavioral response to a limited free space on the pond in which to skim. This concept is supported by a simple count of how many birds are present in the volume of interest at the moment of impact for each landing. The distribution of those counts are significantly different between the groups (Pearson two-tailed T-Test, $p < 0.05$) with mean numbers of birds in the vicinity at 9 and 13 correspondingly for typical and atypical landings.

In addition, if atypical landings are a response to an external signal then the typical landings may be more representative of the preferred landing strategy of mallards. This is particularly interesting as the typical group has faster landing speeds and shallower angles, which would strengthen the evidence that the approach kinematics used to land on water have deviated in a consistent direction from what we know of perch landing kinematic in pigeons (Green and Cheng, 1998).

3.5 *Conclusions*

This study has examined the landing kinematics of mallards landing on water and looked at how the approach kinematics may influence a resulting kinematic of water landings, the distance traveled after impact. The data showed that there is a large degree of variation within the distance after impact that a mallard may travel with a range of 0 – 6.04 m having been observed (Table 3.2). This variation is correspondingly matched by large ranges in all the approach kinematics and each of these kinematics has some predictive ability for distance after skimmed based on regression analyses (Figure 3.2). However, a combination of GLM's, PCA, and clustering suggests that only three approach kinematics, horizontal impact velocity, impact

angle, and mean approach angle are drivers of distance after impact, suggesting they may be key parameters ducks may track and regulate to land. In addition, of those three parameters horizontal impact velocity is by far the primary kinematic influencing these landing behaviors as it's coefficient in the model is an order of magnitude greater that of either impact angle or mean approach angle. Last, a K-cluster analysis was done on a PCA analysis of kinematic profile based on the three key approach kinematics found. The results suggested a delineation within the data which can be categorized as typical landings and atypical landings. The typical landings are the majority of landings observed (N=119) and imply that most mallards land on water with relatively high impact speeds and at shallow angles. These are distinct from the much steeper and slower landing that have been documented for perch landings in pigeons (Green and Cheng, 1998). Mallards will land at slower speeds and with steeper angles though these atypical landings (N=58) are less common. The cause of atypical landings is not clear, though it seems likely due to how the kinematics shift from typical to atypical and the higher likelihood of more ducks already being in the water when an atypical landing occurs. Thus, these landings may be tied to an obstacle and collision avoidance adaptation of a mallard's typical landing strategy.

3.6 *References*

Berg, A. M. and Biewener, A. a (2010). Wing and body kinematics of takeoff and landing flight in the pigeon (*Columba livia*). *J. Exp. Biol.* **213**, 1651–8.

Bergou, A. J., Swartz, S. M., Vejdani, H., Riskin, D. K., Reimnitz, L., Taubin, G. and Breuer, K. S. (2015). Falling with style: Bats perform complex aerial rotations by adjusting wing inertia. *PLoS Biol.* **13**, 1–16.

de Margerie, E., Simonneau, M., Caudal, J.-P. P., Houdelier, C., and Lumineau, S. (2015). 3D tracking of animals in the field using rotational stereo videography. *J. Exp. Biol.* **218**, 2496–2504.

de Margerie, E., Pichot, C. and Benhamou, S. (2018). Volume-concentrated searching by an aerial insectivore, the common swift, *Apus apus*. *Anim. Behav.* **136**, 159–172.

Evangelista, D. J., Ray, D. D., Raja, S. K. and Hedrick, T. L. (2017). Three-dimensional trajectories and network analyses of group behaviour within chimney swift flocks during approaches to the roost. *Proc. R. Soc. B Biol. Sci.* **284**, 20162602.

Fry, S. N., Sayaman, R. and Dickinson, M. H. (2005). The aerodynamics of hovering flight in Drosophila. *J. Exp. Biol.* **208**, 2303–2318.

Green, P. and Cheng, P. (1998). Variation in kinematics and dynamics of the landing flights of pigeons on a novel perch. *J. Exp. Biol.* **201**, 3309–3316.

Hedrick, T. L. and Daniel, T. L. (2006). Flight control in the hawkmoth *Manduca sexta*: The inverse problem of hovering. *J. Exp. Biol.* **209**, 3114–3130.

Jackson, B. E., Evangelista, D. J., Ray, D. D. and Hedrick, T. L. (2016). 3D for the people: multi-camera motion capture in the field with consumer-grade cameras and open source software. *Biol. Open* **5**, 1334–1342.

Johnsgard, P. A. (2010). Tribe Anatini (Surface-Feeding Ducks). In *Ducks, Geese, and Swans of the World* (ed. Nebraska, U. of), pp. 216–219. Lincoln.

Khandelwal, P. C. and Hedrick, T. L. (2020). How biomechanics, path planning and sensing enable gliding flight in a natural environment. *Proceedings. Biol. Sci.* **287**, 20192888.

Lee, D. N., Davies, M. N. O., Green, P. R. and Van Der Weel, F. R. (1993). Visual control of velocity of approach by pigeons when landing. *J. Exp. Biol.* **180**, 82–104.

Ling, H., McIvor, G. E., Nagy, G., MohaimenianPour, S., Vaughan, R. T., Thornton, A. and Ouellette, N. T. (2018). Simultaneous measurements of three-dimensional trajectories and wingbeat frequencies of birds in the field. *J. R. Soc. Interface* **15**, 20180653.

Norberg, R. Å. A. and Norberg, U. M. (1971). Take-off, landing, and flight speed during fishing flights of *Gavia stellata*. *Ornis Scand.* **2**, 55–67.

Ristroph, L., Ristroph, G., Morozova, S., Bergou, A. J., Chang, S., Guckenheimer, J., Wang, Z. J. and Cohen, I. (2013). Active and passive stabilization of body pitch in insect flight. *J. R. Soc. Interface* **10**,.

Ros, I. G., Bassman, L. C., Badger, M. A., Pierson, A. N. and Biewener, A. A. (2011). Pigeons steer like helicopters and generate down and upstroke lift during low speed turns. *Proc. Natl. Acad. Sci.* **108**, 19990–19995.

Theriault, D. H., Fuller, N. W., Jackson, B. E., Bluhm, E., Evangelista, D., Wu, Z., Betke, M. and Hedrick, T. L. (2014). A protocol and calibration method for accurate multi-camera field videography. *J. Exp. Biol.* **217**, 1843–1848.

Tobalske, B. W., Warrick, D. R., Clark, C. J., Powers, D. R., Hedrick, T. L., Hyder, G. A. and Biewener, A. A. (2007). Three-dimensional kinematics of hummingbird flight. *J. Exp. Biol.* **210**, 2368–2382.

Urban, S., Leitloff, J. and Hinz, S. (2015). Improved wide-angle, fisheye and omnidirectional camera calibration. *ISPRS J. Photogramm. Remote Sens.* **108**, 72–79.

Vejdani, H. R., Boerma, D. B., Swartz, S. M. and Breuer, K. S. (2019). The dynamics of hovering flight in hummingbirds, insects and bats with implications for aerial robotics. *Bioinspiration and Biomimetics* **14**.

Wolf, M., Johansson, L. C., Von Busse, R., Winter, Y. and Hedenström, A. (2010). Kinematics of flight and the relationship to the vortex wake of a Pallas' long tongued bat (*Glossophaga soricina*). *J. Exp. Biol.* **213**, 2142–2153.

Wolf, M., Ortega-Jimenez, V. M. and Dudley, R. (2013). Structure of the vortex wake in hovering Anna's hummingbirds (*Calypte anna*). *Proc. R. Soc. B Biol. Sci.* **280**,.

Yu, B., Gabriel, D., Noble, L. and An, K. N. (1999). Estimate of the optimum cutoff frequency for the Butterworth low-pass digital filter. *J. Appl. Biomech.* **15**, 318–329.

Zhang, Z. (2000). A flexible new technique for camera calibration. *IEEE Trans. Pattern Anal. Mach. Intell.* **22**, 1330–1334.

Chapter 4

Mallards avoid obstacles when landing on water

Abstract

The ability of flying animals to navigate obstacles in their environment has been documented in a host of different animals at large and small scales of locomotion. Here, we examine if mallards demonstrate similar obstacle avoidance behavior when landing on water. To test for this behavior, the natural variation in the number of other waterfowl in the landing area, and a predicted landing strip, was leveraged to see if mallard landing behavior skim distance would be lower when the number of other waterfowl was higher. However, analyses showed that out of 177 landings only 5 landings had another waterfowl in the landing strip. This occurred despite there being other waterfowl within the wider landing area for 165 landings. Therefore, to further test if this was evidence of strong avoidance of obstacles in a mallards landing path two simulations were run to see if the mallards avoided obstacles better than chance. The random simulation reassigned the heading, direction angle at impact, for each landing a new random angle between 1° - 360°. The shuffle simulation reassigned headings performed by mallards at this pond to a different, unrelated landing event. The results of the simulations demonstrated that the landings with shuffled headings performed significantly better than chance. This implies that mallards are avoiding obstacles, such as other waterfowl, when landing. However, due to how the shuffle simulation reassigned headings, it is unclear if this avoidance is an active behavior on the part of the mallard. The observed results may arise from habitual landing and congregation patterns of the mallards and waterfowl in the water, thereby precluding the need for active obstacle avoidance behavior.

4.1 *Introduction*

When navigating ones' local environment animals regularly have to contend with obstacles. These can be comparatively large obstacles such as islands and peninsulas in the case of foraging shearwaters (Padget et al., 2019), or the trees a *Draco* lizard must bank around to reach its intended destination (Khandelwal and Hedrick, 2020). More often, they are smaller rocks and plants which commonly clutter most environments. Effectively navigating a cluttered environment for many terrestrial and arboreal organisms includes climbing and gap crossing (Graham and Socha, 2019). However, for flyers the problem is infrequently a gap you must cross or object you must go over, but an obstacle you must avoid (Sarmiento and Murphy, 2018) . Flight based obstacle avoidance behaviors have been documented in insects (Mongeau et al., 2018), bats (Kugler et al., 2016), and birds (Vo et al., 2016), all of which are capable of aerial maneuvers designed to prevent collision with an obstacle.

For flyers, avoiding clutter can take on different forms. For instance, budgerigars (parakeets) demonstrate the ability to slip between small gaps, which is likely advantageous in navigating the cluttered environment within the branches of trees (Bhagavatula et al., 2011). Brazilian free-tail bats (Kloepper and Bentley, 2017) and chimney swifts (Evangelista et al., 2017), participate in large-scale flock behavior in which they must navigate the dynamic movement of the flock and navigate into their roosts in caves, trees, and chimneys. Waterfowl have a similar, though arguably less complicated task. Due to the tendency of many waterfowl to flock, and do so in large numbers, these birds have to avoid colliding with other waterfowl who are frequently present on the surface of the water, where they are attempting to land.

This is complicated by the fact that waterfowl prefer to skim when they land and the distance of that skim can be several body lengths. As a result, waterfowl may prefer larger landing areas if they are to avoid a collision.

This study examines if mallards exhibit behaviors that may prevent such collisions. To test if mallards avoid obstacles when landing we used the natural obstacles, other waterfowl. Other waterfowl are present to varying degrees during most landings and create a natural experiment upon which to examine the possibility that mallards avoid landing where they may collide with other waterfowl. The likelihood that mallards employ obstacle avoidance behavior is suggested by Chapter 2, which demonstrated that mallards regulate landings utilizing the same collision avoidance strategy based in optic flow utilized by pigeons, bats, and hummingbirds. Next, in Chapter 3 it was shown that the landing kinematics of mallards favor high-speed, shallow landings over slower, steeper ones. However, the steeper landings occur more frequently when there are more waterfowl present in the vicinity. Combined, these findings imply kinematic regulation in response to the nearness of the landing surface and a preference to carry out landings which enable a longer skim. Therefore, mallards may regulate landing kinematics to avoid a collision with another duck already in the water and/or give them the space to skim. If mallards regulate landing kinematics based on other waterfowl, we would expect to see a negative relationship between distance after impact and the number of waterfowl in the vicinity or landing area. This would imply the mallard is skimming less when the area is crowded to avoid collisions. However, mallards may simply land where the other waterfowl are not. This would mean that within a broader landing area, the specific region in which a mallard lands would have a lower occurrence of other waterfowl.

4.2 *Methods*

To find the proximity of all waterfowl, not just mallards, present for a given landing event videos were collected from three video cameras (GoPro HERO4 Black), on wide view at 4k and 30 fps, spaced along one side of the pond. The cameras were synced post-hoc based on sound pulses from radios attached to the tripod of each camera, optical distortion was removed from the resulting videos based on omnidirectional coefficients (Jackson et al., 2016; Scaramuzza et al., 2006b), and the volume of interest (VOI) was calibrated using a 0.94 m wand (Jackson et al., 2016; Zhang, 2000). The resulting calibration had maximum wand length error of ± 2.18 cm. Further details on methods can be found in Chapter 2.2.

In these videos the time of initial impact was re-examined for all landings and at that moment all birds that were already in the water and could be seen from multiple GoPro

cameras were digitized. From this digitization the position in the xy-plane could be found and the distance with respect to position of the initial impact calculated. However, all birds in the water that can be seen is a very broad category and many of those individuals may not be pertinent to a given landing event. Therefore, waterfowl were considered relevant to a landing event if the individual was less than or equal to 6.02 m away from the point of initial impact. This number was based on the maximum distance skimmed of any mallard in the dataset. This value was used to define a circular landing area around the point of initial impact with a radius of 6.02 m (Fig 4.1A). To implement this the point of initial impact was made the origin for each landing event, transforming the positions of all other individuals present accordingly.

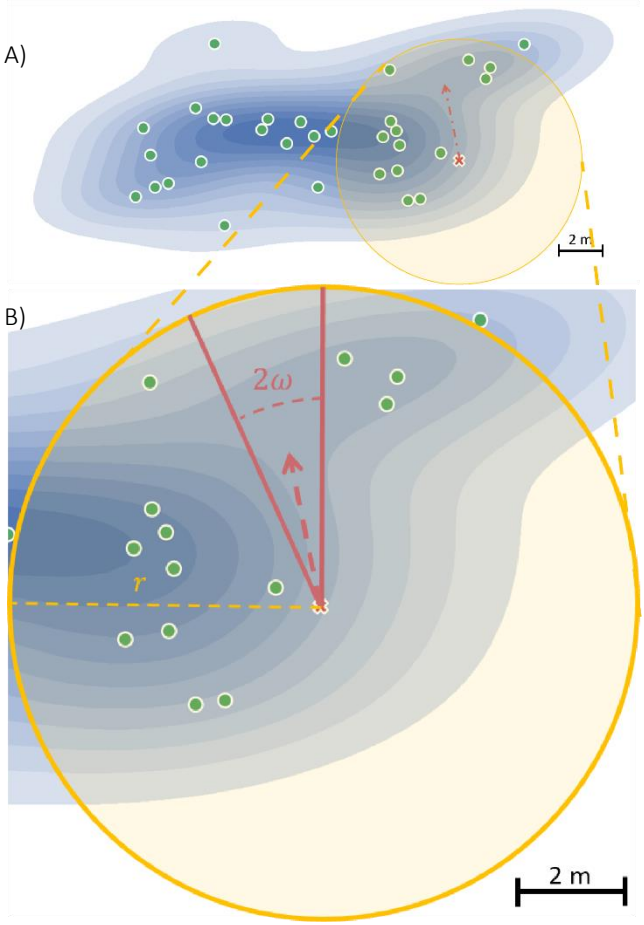

Figure 4.1: How the landing area and landing strip are defined. An example of a distribution of waterfowl across the water surface as seen from above. The waterfowl are shown as green circles while the point of initial impact of the landing mallard is marked with a red 'x'. The direction of the mallard's horizontal velocity at impact is shown by the red arrow. The blue shaded regions are a bivariate KDE of the distribution of waterfowl on the surface. Dark blue represents a higher relative density of waterfowl while lighter shades represent a lower relative density of waterfowl. The whole distribution of all waterfowl seen by the camera and the 6.02 landing area (yellow circle) derived from maximum skim distance of a mallard is shown in A. If the landing area is zoomed in on, B, the parameters used to create a landing strip around the horizontal velocity vector at impact are shown. The radius (r = 6.02 m) of the landing area is shown as is the resulting slice of the landing area (2ω = 24°) bisected by the direction of the horizontal velocity to create a landing strip, where ω is the standard deviation of the angles of deviation from a straight skim observed.

Then, all individuals whose hypotenuse, based on their x and y coordinates, exceeded 6.02 meters were removed from the analysis. However, each landing has a heading, or direction in which the mallard is traveling at impact, and those individuals in front of the duck are likely to have more impact on landing behavior than those behind. Therefore, a narrower landing strip was calculated with respect to each mallard, creating a potential landing strip in which a mallard may skim after impact. The angle for this landing strip was defined as twice the standard deviation of the observed divergence from the impact heading. That is the difference between the impact heading angle, derived from horizontal impact velocity, and the line created by connecting the point of initial impact to the end point of the skim. This angle would also be the angle of the arc between a straight skim based on the impact heading and the actual end position, as there can be a slight curve to any given skim. The mean deviation from impact heading is 8° ± 12°, therefore the landing strip of each landing event was given an arc with an angle twice the standard deviation, 24°. This arc was positioned so that the landing strip created was bisected by the impact heading (Fig 4.1B). This was implemented by dropping any waterfowl, of those within the landing area, whose arc angle with respect to the impact heading was either greater than 12°or less than -12°.

Based on this hypothesized landing strip a Pearson's r test was run on the number of waterfowl for each landing event compared to distance after impact. In addition, of those landings which did have other waterfowl within the landing strip, the distance to the nearest potential obstacle (other waterfowl) was plotted with respected to distance after impact.

Last, two simulations were created to test if the landing headings of the mallards limit the number of obstacles (i.e., individuals) in a landing strip better than chance. The first was a

random heading simulation. The impact headings observed were discarded for this simulation and in place of them a random angle between 1° and 360° was assigned to each landing event. The position of all other waterfowl and the point of initial impact were retained for each landing event, but the simulated mallard is now skimming in a randomized different direction, hence this is called the random simulation. The second simulation also kept all factors the same except for impact heading. However, instead of assigning random headings, a heading angle from all the landing events observed was randomly selected. In essence, all headings were shuffled so that the simulated mallard has a heading that is an actual behavior observed by the mallards, but different from what the mallard actually did. Each simulation was run 1000 times, the number of individuals in the landing strip was found for each simulated landing, and the average number of individuals in the landing strip out of all the simulations for each landing event was calculated. The distributions of average number of individuals in the landing strip could then be compared between the two different simulations and tested for significant differences through two-tailed t-test.

4.3 *Results*

A relationship between the distance after impact and the number of individuals in the landing strip (Fig. 4.2A) is not present (Pearson linear regression, $p > 0.05$). However, predicted correlations do not exist because 172 of 177 landing events recorded have no ducks in the landing strip, leaving only 5 landing events with any individuals present in the landing strip. This lack of individuals is not a feature of there not being other waterfowl in the vicinity. There is only one landing in the dataset of 177 landing events in which there are no other individuals already present in the water. Also, in the larger landing area (Fig. 4.2B) there are only 12 landing events without at least one individual present in the 6.02 m circle around impact. In other words, at this site there is one other individual in the pond 99% of time and for a given

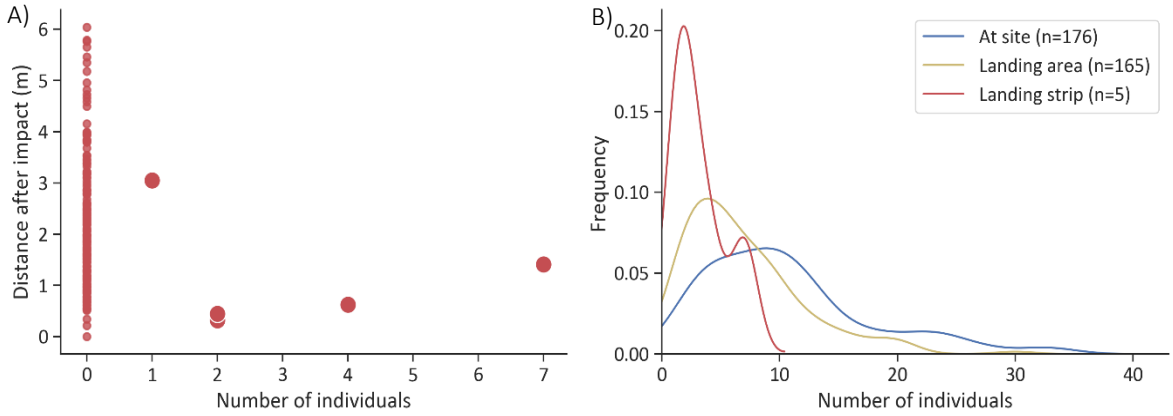

Figure 4.2: Number of individuals in the landing strip compared to distance after impact and the normalized frequency distributions for the number of individuals at the site, landing area, and landing strip when that number is not zero. Based on the defined landing strip there is no correlation between the number of individuals present and the distance traveled after impact ($p > 0.05$), shown in A, probably due to the fact the vast majority of landings, 172 out of 177, have no individuals in the landing strip. For all landings in which the number of individuals present was not zero at the site (blue), the landing area (yellow), and landing strip (red) were all plotted based on KDE (kernel density estimates) in B. The distributions show the probability of a certain number of individuals being present in that area, if any individuals are present. In addition, the total number of landings in which an individual is present is shown in the key. These n values show that only one landing in the dataset has no individuals in the water at the site and within the more limited landing area, there are still only 12 in which an individual is not present. This lack of high numbers of zero individual landing events when examining the whole site and the landing area demonstrate that the lack of individuals in the landing strip is not an artifact of there simply not being individuals in the vicinity.

landing there is a 93% chance there are other individuals within 6 meters of where the mallard lands. The mean number of individuals at the broader site was 10 ± 7 individuals, while the number within the landing area is 6 ± 5 individuals. The drop in number of landings with other individuals in the landing strip is quite precipitous, 93% to just below 3%. Those 5 landings in which there are individuals within the landing strip can be examined more closely based on the distance to the nearest neighbor. The distance to the nearest neighbor for each of these landings, Figure 4.3, is near equal to or higher than the distance skimmed by the subject. This can be clearly seen based on the green dashed line denoting a threshold at which the distance to the nearest neighbor and the distance after impact are the same. Any points above that line are skims that went far past the nearest neighbor in the landing strip and may have been landings with a higher risk of collision. Meanwhile, points below or on the line would be skims in which the mallard is stopping well before the nearest neighbor or skimming up near or alongside their nearest neighbor. For these 5 landings none of the distances traveled after impact are substantially higher than the distance to the nearest neighbor. Two are significantly below a 1:1 relationship, both skimming no more than 1 m while the nearest neighbor is 3 and 4 meters

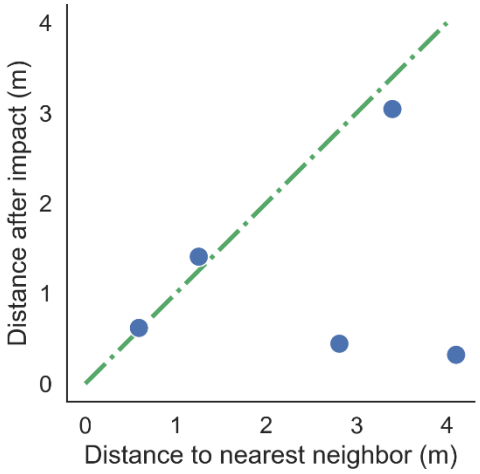

Figure 4.3: Of the five landings in which there is at least one individual in the landing strip the distance to the nearest neighbor was examined with respect to distance after impact. The green dashed line represents a 1:1 relationship between the two variables. Therefore, any point above the line is a potential collision due to skimming which went far past the position of the neighbor, below the line is a skim that stops before reaching the neighbor, and on or near the line are skims that stop at or near the neighbor. For these five landings in which there are individuals in the strip two stop well before the nearest neighbor, while the other three stop right near the line.

away respectively. The other three are on or near the line, suggestive they are skimming up to or near the nearest neighbor.

The combination of a precipitous drop in other individuals present in landing strips compared to the broader landing area and the fact that in the five cases in which individuals were present travel distance were shorter than those that could lead to higher velocity collisions is suggestive of non-random landing behavior. However, with the creation of the landing strip we have also greatly diminished the area in which individuals could be an obstacle. As a given landing area has relatively few individuals in it (6 ± 5) the density of obstacles for any given landing is actually quite low, 0.06 ± 0.04 individuals per square meter. It is therefore plausible the mallards could land completely randomly and rarely run into another waterfowl.

To test if mallard landing behavior avoids potential obstacles at a rate better than chance two simulations were run. One simulation had randomized impact headings, the random simulation, and the second simulation had actual impact headings of mallards shuffled to random landing events, the shuffle simulation. The average number of individuals present in the landing strip for each landing event in both simulations was calculated from 1000 iterations. Then, the distributions of those average counts could be compared using a two-tailed T-test for independence. The results showed that headings used by mallards had a significantly lower average number of individuals in any given landing strip ($p << 0.001$). The frequency of average numbers of individuals in a landing strip can be seen for both the shuffled and randomized models in Figure 4.4A, where the shuffled simulation shows a much higher frequency of lower average numbers below 0.5 individuals in a landing strip. The significant difference between the results of the simulations can be clearly seen once the distributions are log transformed (Fig

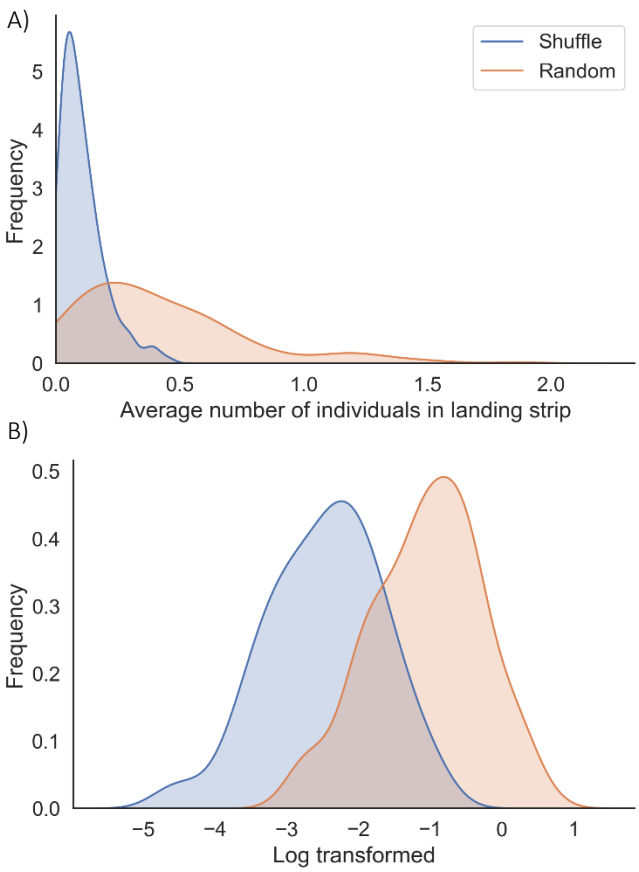

Figure 4.4: Mallard impact headings limit the number of individuals in the landing strip compared to random headings. The shuffle simulation shuffles all impact headings observed in mallards and randomly assigns them to new landing events. The random simulation assigns a completely new random angle from between 1° to 360° for each landing event. The average number of individuals found in all landing strips simulated for each landing event was calculated; the results are shown in A. To ensure the shuffle simulation did create a different distribution for average number of individuals in a landing strip, the distributions were log transformed, B, and a two-way T-Test found the results to be significantly different ($p << 0.001$).

4.4B). There is clear significant downward shift in the numbers of individuals in a landing strip for landings in which the headings are from actual landing events at the pond.

4.4 *Discussion*

The results have shown that for mallards to land on water there is some level of landing strip selection. The low number of landings in which mallards land with at least one other individual in the landing strip combined with the lack of potentially high velocity collisions present when there are individuals in the landing strip imply a behavioral selection of landing strip. The shuffle simulation compared to random demonstrates that these low numbers of landings with individuals in a landing strip is not chance, further supporting the hypothesis that mallards are selecting a landing strip. However, the shuffle simulation is randomly assigning a heading from an actual mallard to a different instance in time with respect to the position of all other

waterfowl on the pond, so why does this simulation perform better than chance? A likely reason for this is that many animals, including birds (Brown, 1963), are quite habitual when it comes to moving throughout the environment. Therefore, the waterfowl on the pond may congregate in consistent locations, thereby inadvertently creating consistent landing strips across time at this site. The likelihood of this behavior is also increased by the methods of this study which involved feeding cracked corn to attract landing waterfowl, which inherently creates a concentration of birds on one side of the pond and may also incentivize landing mallards to have more consistent impact headings. The natural inclination of the ducks to approach and interact on the pond similarly and the feeding within the methodology of this study could combine to create highly analogous landing situations for most mallards.

4.5 *Conclusions*

As might be expected based on the prevalence of avoidance behaviors seen for flight broadly (Sarmiento and Murphy, 2018) mallards do participate in avoidance behaviors with regards to other waterfowl in the vicinity of landing. Interestingly, this study suggests the ducks have a very strong preference to land so that other waterfowl are simply not in the way, though they appear to be able to regulate landing if others are in the landing strip. However, it is hard to say with confidence how the mallards interact when others are in the landing strip as it only happened in 5 landing events in a dataset of 177. Importantly, due to the low density of birds in the region overall simulations demonstrate that the landing behavior of the mallards does avoid obstacles better than random chance.

4.6 *References*

Bhagavatula, P. S., Claudianos, C., Ibbotson, M. R. and Srinivasan, M. V. (2011). Optic flow cues guide flight in birds. *Curr. Biol.* **21**, 1794–1799.

Brown, R. (1963). The flight of birds. *Biol. Rev.* **38**, 460–489.

Evangelista, D. J., Ray, D. D., Raja, S. K. and Hedrick, T. L. (2017). Three-dimensional trajectories and network analyses of group behaviour within chimney swift flocks during approaches to the roost. *Proc. R. Soc. B Biol. Sci.* **284**, 20162602.

Graham, M. and Socha, J. J. (2019). Going the distance : The biomechanics of gap - crossing behaviors. *J. Exp. Zool.* 1–14.

Jackson, B. E., Evangelista, D. J., Ray, D. D. and Hedrick, T. L. (2016). 3D for the people: multi-camera motion capture in the field with consumer-grade cameras and open source software. *Biol. Open* **5**, 1334–1342.

Khandelwal, P. C. and Hedrick, T. L. (2020). How biomechanics, path planning and sensing enable gliding flight in a natural environment. *Proceedings. Biol. Sci.* **287**, 20192888.

Kloepper, L. N. and Bentley, I. (2017). Stereotypy of group flight in Brazilian free-tailed bats. *Anim. Behav.* **131**, 123–130.

Kugler, K., Greiter, W., Luksch, H., Firzlaff, U. and Wiegrebe, L. (2016). Echo-acoustic flow affects flight in bats. *J. Exp. Biol.* **219**, 1793–1797.

Mongeau, J.-M., Cheng, K. Y., Aptekar, J. and Frye, M. A. (2018). Visuomotor strategies for object approach and aversion in *Drosophila melanogaster*. *J. Exp. Biol.* **222**, jeb193730.

Padget, O., Stanley, G., Willis, J. K., Fayet, A. L., Bond, S., Maurice, L., Shoji, A., Dean, B., Kirk, H., Juarez-martinez, I., et al. (2019). Shearwaters know the direction and distance home but fail to encode intervening obstacles after free-ranging foraging trips. *Proc. Natl. Acad. Sci.* **10**, 1903829116.

Sarmiento, T. A. and Murphy, R. R. (2018). Insights on obstacle avoidance for small unmanned aerial systems from a study of flying animal behavior. *Rob. Auton. Syst.* **99**, 17–29.

Scaramuzza, D., Martinelli, A. and Siegwart, R. (2006). A toolbox for easily calibrating omnidirectional cameras. *IEEE Int. Conf. Intell. Robot. Syst.* 5695–5701.

Vo, H. D., Schiffner, I. and Srinivasan, M. V. (2016). Anticipatory manoeuvres in bird flight. *Sci. Rep.* **6**, 1–8.

Zhang, Z. (2000). A flexible new technique for camera calibration. *IEEE Trans. Pattern Anal. Mach. Intell.* **22**, 1330–1334.

Chapter 5

The kinematics and behavior of mallards landing on water

5.1 *Conclusions*

This dissertation examined how mallards regulate flight kinematics when landing on water. In particular I examined the following questions: i) Do mallards use the same regulatory strategy that has been observed in animals landing on a perch? ii) How variable are the kinematics of how mallards land on water? Are there different types of landings contained within that variation? iii) Is there a degree of plasticity in the kinematics in response to how crowded the landing is? With photogrammetric techniques that utilized two separate camera systems, 177 landing trajectories of mallards and the kinematics of the transition into the water were tracked in three dimensions. From the trajectory and transition data, a number of features related to landing were identified. To assess how mallards regulate landing kinematics, the regulatory parameter τ was calculated for each landing. To examine the variation present in landing on water, horizontal impact velocity, vertical impact velocity, impact angle, mean approach angle, distance after impact, transition duration, and range of motion of body were all calculated as comparative kinematic parameters with which to describe the landings. To test how crowding influences landing kinematics, the position of other waterfowl present for each landing was also determined. These analyses revealed that: i) Mallards use the same $\dot{\tau}$-constant landing strategy to land on water as seen in pigeons, hummingbirds, bats, and *Draco* lizards landing on solid substrates (Khandelwal and Hedrick, 2020; Lee et al., 1991; Lee et al., 1993; Lee et al., 1995). ii)

There is a broad array of kinematic profiles with which mallards can land on water; however, the primary driver of the landing outcomes on water is horizontal impact velocity. In addition, there are no dramatically distinct types of landings, but there is evidence of a consistent kinematic profile that is typified by shallow, high velocity kinematics. The remaining landings have kinematic profiles that are more disparate from each other, but can be typified by steeper, slower velocity kinematics. iii) Mallards do not land where other waterfowl are likely to become obstacles; however, it is not clear if this avoidance is due to behavioral plasticity on the part of mallard or arises from external factors.

The results from Chapter 2 and 3 illustrate a landing behavior performed by mallards which is kinematically similar to perch landing in pigeons, but is implemented differently. Mallards regulate landings using the same strategy, but the higher mean value of $\dot{\tau}$ implies an adjustment to how the strategy is implemented. Mallards do land on water with different kinematics. The typical landing of mallards on water is both shallower and faster than a pigeon landing on a perch, which results in the maximum momentum experienced by a mallard at impact being up to an order of magnitude greater than what is experienced by pigeons. However, the distributions of landing kinematics do overlap, and the atypical landings performed by mallards suggest that their landing behavior is plastic enough to perform landing kinematics highly similar to that seen in landing pigeons.

These results are similar to what has been found in regard to flight kinematics due to changes in altitude. As air density is a fundamental constraint upon the generation of lift, birds should need to adjust to the reduced density of the air to maintain typical flight performance (Alexander, 1983). This concept has been particularly well tested with hummingbirds at

different air densities, and there are changes in how the bird flies (Altshuler and Dudley, 2003). However, these are not dramatic changes in which the flight behavior is a different mode of flight. Instead the birds make kinematic adjustments by increasing both wing stroke frequency and amplitude, thereby generating more lift (Altshuler and Dudley, 2003). However, while these kinematic adjustments are made on small time scales, prolonged changes in air density can lead to morphological changes within and across species (Altshuler et al., 2010; Sun et al., 2016). Changing the landing substrate to water may be similar. Mallards do not have a dramatic change in landing behavior, but make kinematic adjustments that utilize the greater force absorptive properties of the new substrate. This behavior is particularly evident in the typical water landing kinematics, which is shallow and fast. This landing preference implies a behavioral shift for less braking in the air, because the water will dissipate the impact forces. It is currently unclear if the shift seen in kinematics to land on water has resulted in morphological changes to waterfowl species, as altitude has in other flyers, as other selective pressures from swimming, dabbling (how mallards and related ducks feed), and diving are likely to be more prevalent. However, this is one potential avenue of further research.

The results from Chapter 4 are less clear with regards to the broader landing behavior of mallards. The significant difference between the results of the shuffled landing headings and random headings suggest the mallards are not randomly landing on the pond regardless of the position of other waterfowl on the pond. However, as the shuffled simulation has shuffled the headings independent of landing conditions, it suggests that the specific conditions of the landing area are fairly homogenous across landings. Therefore, it is not clear if mallards are actively avoiding these potential obstacles or if it is a feature that arises from the geography of

this locality and habits of this population. Based on how Chapter 2 and 3 demonstrate a general conservation of landing ability compared to perch landing and the prevalence of flight based object avoidance behaviors in birds (Bhagavatula et al., 2011; Lin et al., 2014; Sarmiento and Murphy, 2018), some level of obstacle avoidance or path planning should be expected. Further studies are needed to confirm their presence in mallard landing behavior.

5.2 *Future work*

There are several avenues highlighted by the results of this dissertation that warrant further study.

5.2.1 *What are the detailed kinematics of a mallard during a skim? How do mallards balance the torques experienced when landing on water?*

This dissertation has assessed the landing behavior of mallards based primarily on the kinematics of the approach under the assumption that the landing impact and result will largely depend on those approach kinematics. However, in Chapter 3 it became apparent this is not true. While the approach kinematics are relevant, based on distance after impact, the approach kinematics only explain approximately 25% of the variation observed in the results of landings. An experiment, using a long flume with reared and trained ducks would enable recording of the landing impact and more importantly the kinematics of a skim above and below the water. This set-up will help ascertain how shifts in a mallards' center of mass during the transition may effect a skim. Also, it could reveal whether the breast and feet are shaped so as to act as planes for lift and drag, and if and how ducks paddle their feet during a skim.

5.2.2 *How does one species of duck adjust their landing kinematics across substrates of different compliance?*

A direct comparison of how a species of waterfowl lands on substrates of varying compliance is needed. This dissertation established that, broadly speaking, a change in a substrate's compliance will lead to changes in the landing kinematics of a bird. However, it has not clearly assessed how a single bird adjusts its kinematics based on changes in substrate compliance. A good study species for such an endeavor would likely be a wood duck (*Aix sponsa*). Wood ducks nest in trees; therefore, a comparison could be made between landing on solid ground, water, and perches of varying compliance. The experiment would require a laboratory or outdoor facility in which the ducks could be trained to fly and land on each substrate. This experiment would have the benefit of making kinematic analysis of photogrammetric techniques easier, and the recordings could have much greater resolution than recording the behavior in field.

5.2.3 *Do mallards actively avoid increased crowding on a pond for landing?*

Chapter 4 demonstrated that mallards avoid landing where obstacles, i.e., waterfowl, would be in the way significantly better than chance. However, it did not prove that this result is an active avoidance strategy. To assess this question effectively, experimental manipulation of the landing conditions and a collection of landing trajectories from various different ponds would be useful. Tracking of landing behavior at multiple ponds and the position of waterfowl during landing on those ponds will clarify if there are site-specific factors contributing to the strong pattern of obstacle avoidance seen in this dissertation. In addition, the presence and absence of obstacles at a pond should be manipulated. These obstacles should be both inanimate objects,

buoys, and waterfowl decoys. This would enable the experimenter to manipulate the timing, position, and concentration obstacles on the water surface. By manipulating these three parameters and the type of obstacle, buoy or decoy, the experiment could answer several questions. Do mallards react differently to simple obstacles than they do to decoys (other waterfowl)? How relevant is habituation to how a mallard lands? If an arrangement of obstacles is novel is there a greater variety observed in the landing headings? If the distribution of obstacles is continuous for a period of time, do the birds convene on a fewer number of headings?

5.2.4 *Does a change in preferred or typical landing substrate compliance lead to morphological changes?*

This would be a long-term study. The landing behavior for number of dabbling ducks, family Anatidae, would be recorded. For a significant diversity of species in Anatidae, important landing kinematic parameters (horizontal impact velocity, impact angle, and mean approach angle) and the preferred $\dot{t}$ would need to be documented. Then, detailed morphometrics for each of these species would need to be collected, either from a literature review, survey data (USFWS), or collected from museum specimens. These morphometrics would need to include mass, body length, wing chord length and wing span, length of digits, and degree of webbing. Other features, such as buoyancy would also be useful. Once all of this information is in hand, a scaling analysis could be done to see if there are any strong relationships between landing kinematics and morphology within a family of waterfowl.

5.3 *References*

Alexander, R. M. (1983). Motion in fluids. In *Animal mechanics*, pp. 183–236. Funtington: Blackwell Scientific Publications.

Altshuler, D. L. and Dudley, R. (2003). Kinematics of hovering hummingbird flight along simulated and natural elevational gradients. *J. Exp. Biol.* **206**, 3139–3147.

Altshuler, D. L., Dudley, R., Heredia, S. M. and McGuire, J. A. (2010). Allometry of hummingbird lifting performance. *J. Exp. Biol.* **213**, 725–734.

Bhagavatula, P. S., Claudianos, C., Ibbotson, M. R. and Srinivasan, M. V. (2011). Optic flow cues guide flight in birds. *Curr. Biol.* **21**, 1794–1799.

Khandelwal, P. C. and Hedrick, T. L. (2020). How biomechanics, path planning and sensing enable gliding flight in a natural environment. *Proceedings. Biol. Sci.* **287**, 20192888.

Lee, D. N., Reddish, P. E. and Rand, D. T. (1991). Aerial docking by hummingbirds. *Naturwissenschaften* **78**, 526–527.

Lee, D. N., Davies, M. N. O., Green, P. R. and Van Der Weel, F. R. (1993). Visual control of velocity of approach by pigeons when landing. *J. Exp. Biol.* **180**, 82–104.

Lee, D. N., Simmons, J. A., Saillant, P. A. and Bouffard, F. (1995). Steering by echolocation: a paradigm of ecological acoustics. *J. Comp. Physiol. A* **176**, 347–354.

Lin, H.-T., Ros, I. G. and Biewener, A. A. (2014). Through the eyes of a bird: modelling visually guided obstacle flight. *J. R. Soc. Interface* **11**, 20140239–20140239.

Sarmiento, T. A. and Murphy, R. R. (2018). Insights on obstacle avoidance for small unmanned aerial systems from a study of flying animal behavior. *Rob. Auton. Syst.* **99**, 17–29.

Sun, Y.-F., Ren, Z.-P., Wu, Y.-F., Lei, F.-M., Dudley, R. and Li, D.-M. (2016). Flying high: limits to flight performance by sparrows on the Qinghai-Tibet Plateau. *J. Exp. Biol.* **219**, 3642–3648.

Appendix A

Supplemental information - Mallard landing behavior follows a $\dot{\tau}$-constant braking strategy

Code repository

Python code to process 3D tracked position points, extract kinematics, τ analysis figures, and generate corresponding figures is located at:

https://github.com/TheSochaLab/Mallard-landing-beahvior-follows-a-tau-constant-braking-strategy

A.1 Procedure for recording in the field with GoPro's

Camera set up and calibration

Camera positions were placed along the west shoreline of the filming cove. One camera was aligned near the bridge to look across and up the cove. Any duck that landed in the cove was seen by this camera. A second camera was aligned where the shore begins to bends further west (approximately 10 meters up shoreline from first), and looks across the cove. All ducks except those that land right by the bridge could be seen by this camera. A third camera was aligned where the cove begins to open up (approximately 10 meters along shoreline from second), and looked slightly back into the cove. This view gave a clear profile view of most ducks during their approach to cove while still retaining a clear view the landing. Cameras were synced to a remote control (WiFi Smart Remote, GoPro, Los Angeles, CA, USA), to enable the experimenter to trigger a recording from all three cameras at nearly the same time from a distance. Three radios (2 way radio UHF 400-470 MHz, BaoFeng Radio, Arlington, SD, USA) for *post-hoc* synchronization were attached to the tripod of each camera with Velcro. The fourth radio, used to send beeps, was held by the experimenter.

Once cameras and radios were in place a calibration recording was taken. To calibrate the volume of interest (VOI), the experimenter took the 0.94 m wand, put on waders, and walked into the water from the east shore, where they could be clearly seen by all cameras. Once the recording had begun the experimenter sent three beeps through the radio and held the tip of the wand, above the marker, lightly between two fingers. This position was maintained until the pendulum swinging of the wand stilled and did not move for a count of 10 seconds. The wand in this 10 second window becomes a dipole from which the VOI will be oriented to the gravity axis. Next, the experimenter slowly walked in a large horseshoe pattern from the starting position, near the east shore and bridge, out to the mouth of the cove, then back along the west shore (closer to the cameras). While walking the experimenter always faced the cameras and slowly moved the wand in circles down to the surface of the water then upward above their head. Once the horseshoe pattern was completed a second series of three beeps were emitted from the radios and the recording was ended. When batteries on cameras ran low or the position of the cameras changed for any reason the calibration process was repeated.

Recording

The experimenter would sit approximately 8 meters from the shore. From this position the experimenter retains a clear view of approaches made by ducks while remaining in range to trigger the cameras to record. The cameras were triggered anytime a mallard duck flew over the cove entrance or any other part of the cove. No obvious landing behavior was required to trigger a recording. If a landing did occur, three beeps were sent through the radio as close to end of each landing as possible. To attract ducks to the cove cracked corn was periodically sprinkled on the east shoreline and in the water. When sprinkling corn, cameras were always recording to prevent missed landings. Throughout filming the experimenter would record the wind speed of gusts with a handheld anemometer (WM-2 Ambient Weather handheld weather meter, Chandler, AZ, USA). To measure wind speed the anemometer was held on top of a compass and the combination was slowly rotated until the maximum wind speed and direction was found and recorded. If a top wind speed exceeded 5.4 m/s recording of landings was stopped and any landings from the time of the gust and on were excluded from the dataset.

Days of filming were typically separated by at least one day. If recording was done more frequently the waterfowl would appear to become satiated by the feed. Satiation would lead to much fewer landings as the waterfowl were more likely to swim across the whole pond as opposed to fly across it. This anecdote is supported by the fact that filming was frequently better in cold weather as the ducks were much more aggressive about feed in such weather.

A.2 Procedure for video processing, calibrations, and trajectory digitization

All raw recordings were backed-up to google Gdrive and stored in directories based on date and camera. Videos were cataloged to document the date and whether the video was a calibration, landing event, or other miscellaneous behavior. The catalog documented which cameras a

landing event could be seen from. If a landing event was present in two cameras the video was marked for further processing. All calibration and landing event videos were clipped to include the calibration or landing event and sound synchronization beeps, then exported as mp4 files with matching format to the original (Premiere Pro, Adobe, San Jose, CA, USA).

File naming

When exported all videos were placed into the same directory and renamed with the following format: "[YYYYMMDD]-GP.['Calib' or 'Landing'].[A-Z][01-99][a-z].Cam[01-06]". Where first is the date, followed by 'GP' denoting this a GoPro recording, either 'Calib' for calibration or 'Landing' for landing event and last is order information for the day. The capital letter denotes filming session. A filming session is one consistent calibration set up. The calibrations for a session, for which there can be multiple are labeled 'Calib.A01' and 'Calib.A02' and so on. Any landings that correspond to a given calibration always have the same capital letter, in this case 'A'. This denotes which calibration a given landing is associated with and the numbers that follow increase based on chronological order of the landing events. A video whose name contains 'Landing.C04' occurred during the third filming session of that day and is the fourth landing event of that session. Landing events can have one additional feature. If a landing event has multiple landings in the recording and not enough beeps to make for separate synchronizations the video is duplicated. Then one video receives a lowercase 'a' after its event number and the second receives a 'b'. These letters correspond to the order in which the birds impact the water, not appear on camera. The first duck to hit the water is 'C04a', while the second is 'C04b'. Last, the camera from which this video was recorded is denoted. The cameras were labeled 01 - 06 and so the number of the camera is which camera was used as opposed to position. However, during set up the lowest numbered camera is always closest to the bridge, while the highest is always furthest out along the cove. Therefore, the relative value of the three cameras (low, mid, or high) for a given filming session denotes the perspective of the pond being viewed in a given video.

Removing distortion and the post-hoc synchronization of videos

To ensure accurate tracking of wand and landings the lens distortion due to the fisheye lens of the GoPro's needed to be accounted for. Argus (Jackson et al., 2016) has a built in tool to compensate for the intrinsic distortion of the lens, Dwarp. In addition, Argus has a database of intrinsic parameters for GoPro models and settings of which the HERO4 Black with 4k resolution (fisheye) is included. Therefore, all videos were de-warped based on the distortion parameters supplied by Argus. The exported videos were renamed with the same format as the input except all now have 'dwarp' after the date: "[YYYYMMDD]-dwarp-GP.['Calib' or 'Landing'].[A-Z][01-99][a-z].Cam[01-06]".

Following de-warping the frame offset for each grouping of three videos was found. Argus (Jackson et al., 2016) has another built in tool for synchronization, Sync. To use Sync the videos were uploaded in increasing order of camera number. This means the perspective from

the near the bridge is always the master camera, while the other two perspectives are slaves. Sync can extract and plot the audio track so the experimenter can look for the series of 3 peaks generated by the radio beeps in the audio track of each video. The fraction of time in which the peaks occurred in all three videos was used to narrow Sync's region for matching the audio tracks. In the script, a table will appear showing offset of the two slave cameras in seconds, frames, and the max correlation. This table was saved as a jpeg with the same filename format as the videos, except 'dwarp' is replaced with 'sync' and '-table' is appended to end of filename. In addition, the graph of audio waves generated by Sync is saved following same naming scheme, except '-table' is replaced with '-waves'.

Digitization of calibration and landings

For all digitization, calibrations and landings, the Argus (Jackson et al., 2016) program Clicker was used. The video from the master camera (lowest number camera) was always input first. Followed by the slave cameras in increasing order. As videos are uploaded the frame offset to the master is requested. The frame offset, rounded to the nearest integer, from Sync was input for each video.

First, the wand was digitized in each video when suspended vertically. The corresponding points were then exported with the same filename as the videos, but the 'dwarp' is now 'dipole'. Once this was done the digitization tracks were cleared and each point on the wand was manually digitized every 10 frames. This was done by turning off Auto-advance on Clicker, and skipping forward 50 frames at a time (SHIFT + f). Once through the calibration once, the digitization was started again, but 10 frames forward from the starting frame of digitization. Once the wand was digitized in this way 5 times there was a digitized wand every 10 frames. Wand digitization began with the deliberate movement of the wand in circles and continues until the experimenter completes the horseshoe pattern. This method consistently generated in excess of 100 digitized wands to use for calibration. The files were exported with the 'dwarp' changed to 'digi'. Once digitation was complete the resulting two dimensional points were input into the Argus (Jackson et al., 2016) Wand program. Here, the wand length (0.94) was input, the digitized wand points were uploaded as paired points, and the dipole digitization was uploaded as reference points. The output file follows the standard file format but 'digi' is changed to 'wand'. In addition, the 3D figure of wand points that Wand generates was also saved as a jpeg with a '-figure' appended to the end of the filename for the wand files.

To digitize a landing the videos are input into Clicker same as the calibration videos. All three videos are input in ascending order with the corresponding frame offsets for the slaves, rounded to the nearest integer. Before digitization began, in the options window in Clicker the direct linear transformation (DLT) coefficients that correspond to a given landing's filming session were uploaded. Then, the video was advanced until the moment of initial impact occurred, when mallard first touches the water, and the frame number at this moment was recorded into a digitization catalog for each landing. Once the impact frame for a landing was

identified, the first frame in which the point where the neck and body of the mallard can be seen in at least two videos was located. This is the first digitization point and was recorded as the start frame in the digitization catalog. The landing was then digitized throughout all three videos for every frame in which this point where the body and neck meet could be digitized. Digitization of a landing ended when the skim was complete, which was denoted by the observation a tail wag and/or rearrangement of wings. The last frame digitized is cataloged as the end frame for a landing. Once a landing was completely digitized the points were exported from Clicker where 'dwarp' in the filename was changed to 'digi'. As a result of the DLT coefficients being included in the digitization this export automatically exports 2D points, filename ends in '-xy', and a separate file of 3D points, filename ends in '-xyz'. During digitization additional notes on landings were also made and cataloged. One important example of this is landings which did not land on the water, but did so on the ground were noted as 'Ground' landings in the notes.

A.3 Code for processing and filtering trajectory

All of the 3D points were processed in combination with a digitization catalog which documents the date, video ID, whether it is usable, sex of individual, start frame of digitization, impact frame, and end frame. All processing and filtering was done in Python. First, all landing data was clipped from start to end frame to remove all non-value data points before digitization begins and ends. Next, all not a number values (NaNs) were detected within each landing so the gaps could be interpolated using an unscented Kalman filter based on the `FilterPy` Python package.

Interpolating gaps with unscented Kalman filter

A Kalman filter uses previous positional information of a subject, derives corresponding velocity and acceleration, and uses all three to predict where the subject is most likely to be next. This means that the whole vector in 3D used by the filter is $\vec{x}(t)$ given by

$$\vec{x} = [p_x, v_x, a_x, p_y, v_y, a_y, p_z, v_z, a_z]^T \tag{A.3.1}$$

For this filter a baseline of initial conditions must be supplied and the following was used

$$\overrightarrow{x_0} = [p_x(t_0), 0, 0.1g, p_y(t_0), 500, 0.1g, p_z(t_0), 1000, -0.5g]^T \tag{A.3.2}$$

All initial velocities and accelerations used are in mm/s and mm/s^2 correspondingly. In addition, a measurement function, H was created to allow for the known points to be effectively mapped into the measurement space the filter will use to interpolate missing values.

$$H = \begin{bmatrix} 1 & 0 & 0 & 0 & 0 & 0 & 0 & 0 & 0 \\ 0 & 0 & 0 & 1 & 0 & 0 & 0 & 0 & 0 \\ 0 & 0 & 0 & 0 & 0 & 0 & 1 & 0 & 0 \end{bmatrix} \tag{A.3.3}$$

Therefore, in combination with the measurement function the measurement at any moment in time, t_i, is

$$\vec{x}(t_i) = H \cdot \vec{x}(t_i) \tag{A.3.4}$$

To estimate where the missing points will be a state transition matrix is used. This matrix, F, maps the transition from $\vec{x}(t)$ to later moments in time, $\vec{x}(t + \Delta t)$.

$$F = \begin{bmatrix} 1 & \Delta t & 0.5\Delta t^2 & 0 & 0 & 0 & 0 & 0 & 0 \\ 0 & 1 & \Delta t & 0 & 0 & 0 & 0 & 0 & 0 \\ 0 & 0 & 1 & 0 & 0 & 0 & 0 & 0 & 0 \\ 0 & 0 & 0 & 1 & 0 & 0 & 0 & 0 & 0 \\ 0 & 0 & 0 & 0 & 500 & 0 & 0 & 0 & 0 \\ 0 & 0 & 0 & 0 & 0 & 2g & 0 & 0 & 0 \\ 0 & 0 & 0 & 0 & 0 & 0 & 1 & 0 & 0 \\ 0 & 0 & 0 & 0 & 0 & 0 & 0 & 500 & 0 \\ 0 & 0 & 0 & 0 & 0 & 0 & 0 & 0 & 2g \end{bmatrix} \tag{A.3.5}$$

For these transition states position, velocity, and acceleration are all calculated based on finite differences and the equations of motion

$$\vec{p}(t + \Delta t) = \vec{p}(t) + \vec{v}(t)\Delta t + 0.5\vec{a}(t)\Delta t^2 \tag{A.3.6}$$

$$\vec{v}(t + \Delta t) = \vec{v}(t) + \vec{a}(t)\Delta t \tag{A.3.7}$$

$$\vec{a}(t + \Delta t) = \vec{a}(t) \tag{A.3.8}$$

Measurement noise from the known points was integrated into the interpolation through an uncertainty matrix, R.

$$R = \begin{bmatrix} \sigma_m^2 & 0 & 0 \\ 0 & \sigma_m^2 & 0 \\ 0 & 0 & \sigma_m^2 \end{bmatrix} \tag{A.3.9}$$

The measurement noise used for this analysis was given by the wand calibration done in Argus, which reports a percent variance seen in the wand for a given calibration. This percentage, wand score, can be used to find the noise as a physical distance. Therefore, the measurement noise used for this interpolation was the maximum variance seen for any calibration, $\sigma_m = 21.8\ \mathrm{mm}$. In addition to the noise from the measurement a standardized Discrete Constant White Noise Model where $\sigma^2 = (0.5g)^2$ was applied along all three axes.

$$Q = \sigma^2 \begin{bmatrix} \frac{\Delta t^4}{4} & \frac{\Delta t^3}{2} & \frac{\Delta t^2}{2} \\ \frac{\Delta t^3}{2} & \Delta t^2 & \Delta t \\ \frac{\Delta t^2}{2} & \Delta t & 1 \end{bmatrix} \tag{A.3.10}$$

The last feature needed for an unscented Kalman filter are the Merwe Scaled Sigma Points, which were set to the recommended parameters for this package: $\alpha = 0.001$, $\beta = 2$, $\kappa = 0$. This method was used to interpolate the gaps in the digitization of each landing. Once those

values were interpolated they are smoothed with a Rauch-Tung-Striebal smoothing filter (rts_smoother). Last, those points are used to fill in the gaps in the landings original data to create trajectories with no missing time points.

Butterworth filter used on complete trajectories

With the gaps in digitization filled in the complete trajectories are filtered with a Butterworth filter. A Butterworth filters each individual trajectory by a individualized cutoff frequency, based on the noise present within that trajectory. This is done through selecting an optimum cutoff frequency at an equilibrium between large signal distortions versus low level signal noise based on the root-mean-square (RMS) error of the data when filtered at different frequencies. The RMS error is calculated by (Yu et al., 1999)

$$R(f_c) = \sqrt{{}^{1}/_{N} \sum_{i}^{N} (p_i - \hat{p}_i)^2} \tag{A.3.11}$$

The RMS error can then be plotted across the range of filter frequencies and a cutoff can be found between where the data has high RMS values, large signal distortions included in the data, and low level RMS error values, suggestive of low level noise and higher resolutions filters having diminishing returns. For this data a second order Butterworth was done where the frequency range of cutoffs was 0.1 – 10 Hz with 0.1 Hz increments and a 95% cutoff. This means the following was done for each trajectory. The RMS error values are calculated for a trajectory when filtered across the range of frequencies given. Linear regressions are then repeatedly done for the points sequentially, adding to the data included, starting from 10 Hz (strongest filter) to 0.1 Hz (weakest filter). Once the $r^2 < 0.95$ for the linear regression, the previous frequency is identified as the cutoff frequency which will be the actual filter used on the trajectory. In essence, this technique finds the elbow typically present in the RMS error plots allowing selection of a filter which only removes the largest deviations, most likely to be significant signal distortions, in a given dataset.

Calculate velocity and acceleration

Once position data has been filtered, the velocity and accelerations for each time point were calculated. To accomplish this the 2nd order central, forward, and backward finite differences were calculated based on the corresponding coefficients. Forward difference was used to calculate velocity and acceleration for the first time point in every trajectory

$$v_0 = -1.5p_0 + p_1 - 0.5p_2 \tag{A.3.12}$$

$$a_0 = 2p_0 - 5p_1 + 4p_2 - p_3 \tag{A.3.13}$$

Followed by a backward difference to calculate the velocity and acceleration at the end point in every trajectory

$$v_{-1} = 1.5p_{-1} - 2p_{-2} + 0.5p_{-3} \tag{A.3.14}$$

$$a_{-1} = 2p_{-1} - 5p_{-2} + 4p_{-3} - p_{-4} \quad \text{(A.3.15)}$$

Last, the remaining points between had velocity and acceleration calculated by a central difference

$$v_i = 0.5p_{i+1} - 0.5p_{i-1} \quad \text{(A.3.16)}$$

$$a_i = p_{i+1} - 2p_i + p_{i-1} \quad \text{(A.3.17)}$$

Straighten trajectories into 2-dimensions

After gaps were interpolated and the resulting trajectories had been filtered the data was translated so the approach of all landings was from the same direction and the individual points were rotated in line with the initial approach direction; effectively turning a 3D trajectory into 2D trajectory. To accomplish, first the initial approach angle in the xy plane, μ, is found

$$\mu = -\tan^{-1}\left({}^{p_x}/_{p_y}\right) \quad \text{(A.3.18)}$$

Next, a rotation matrix is created which is defined as

$$M_R = \begin{bmatrix} \cos\mu & -\sin\mu & 0 \\ \sin\mu & \cos\mu & 0 \\ 0 & 0 & 1 \end{bmatrix} \quad \text{(A.3.19)}$$

With this rotation matrix the position of a trajectory can now be iteratively rotated for each sequential point. The dot product of the change in position between two time points, Δp_i, and the rotation matrix gives the displacement from the previous position, p_{i-1}. Therefore, simply add the calculated displacement to previous position to find the coordinates for the straightened trajectory, p_S.

$$p_S = (M_R \cdot \Delta p_i) + p_{i-1} \quad \text{(A.3.20)}$$

Once position has been rotated the non-position variables, velocity and acceleration, must be rotated as well to retain the physical accuracy to what occurs in 3D. Both velocity and acceleration need to be rotated along the yaw axis of the 3D data, therefore the yaw angle, θ, is calculated based on the velocity in the xy-plane

$$\theta = -\tan^{-1}\left({}^{v_x}/_{v_y}\right) \quad \text{(A.3.21)}$$

Which now requires a rotation matrix of its own

$$\theta_R = \begin{bmatrix} \cos\theta & \sin\theta & 0 \\ -\sin\theta & \cos\theta & 0 \\ 0 & 0 & 1 \end{bmatrix} \quad \text{(A.3.22)}$$

with which both velocity and acceleration can be iteratively rotated using the dot product

$$v_S = \theta_R \cdot v_i \quad \text{(A.3.23)}$$

$$a_S = \theta_R \cdot a_i \tag{A.3.24}$$

Extracting kinematic parameters

A number of summary kinematic parameters are extracted from each landing trajectory to enable statistical comparisons. They were horizontal impact velocity, vertical impact velocity, impact speed, impact angle, mean approach angle, and distance after impact. Due to the digitization catalog for parameters such as horizontal and vertical impact velocity are simply extracted from the velocity values in the horizontal and vertical axes at the moment of impact. Impact speed is simply the magnitude of the horizontal and vertical velocity vectors at impact

$$\left|\vec{v}_{imp}\right| = \sqrt{v_{xy}^2 + v_z^2} \tag{A.3.25}$$

Impact angle is extracted from the moment of impact for trajectory angle based on velocity for each moment in time throughout a trajectory

$$\gamma = -\tan^{-1}\left({}^{v_z}/_{v_{xy}}\right) \tag{A.3.26}$$

Mean approach angle is the mean of all trajectory angles up until the moment right before impact. However, this means the point of initial descent had to be selected as well, which was defined as the first moment in a trajectory when $v_z < 0$. Last, distance after impact was calculated by finding the magnitude of the change in distance traveled between each time point during the skim, after which all of those distances were summed

$$d = \sum_{t_{end}}^{t_{imp}} \sqrt{(xy_t - xy_{t+1})^2 + (z_t - z_{t+1})^2} \tag{A.3.27}$$

All kinematic parameters were appended to a Pandas DataFrame of the digitization catalog, so all relevant information for a given trajectory is on a single row for easy comparison and statistical analyses.

Calculating τ and $\dot{\tau}$

To calculate τ you need the distance to the object or collision over the rate of change of that distance. Therefore τ was calculated as the horizontal distance to the point of impact divided by the instantaneous horizontal velocity for each moment in time

$$\tau = \frac{|p_{xy}|}{v_{xy}} \tag{A.3.28}$$

Distance to impact is the horizontal position, p_{xy}, due to the translation of 2D trajectories to align with initial impact. Therefore, the magnitude of the position on the xy-axis for a trajectory is the distance until impact.

To calculate $\dot{\tau}$ we followed the methods of Lee et al. (1993), which calculate $\dot{\tau}$ not as the finite difference of τ, but based on the slope of the best fit linear regression for each landing. Therefore, a SciPy.Stats package in Python was utilized to calculate both the Pearson Linear

Coefficient for the τ of each individual trajectory and a Pearson Linear Regression was implemented. The slopes of each regression were documented as the $\dot{\tau}$ for each individual landing.

A.4 *References*

Jackson, B. E., Evangelista, D. J., Ray, D. D. and Hedrick, T. L. (2016). 3D for the people: multi-camera motion capture in the field with consumer-grade cameras and open source software. *Biol. Open* **5**, 1334–1342.

Lee, D. N., Davies, M. N. O., Green, P. R. and Van Der Weel, F. R. (1993). Visual control of velocity of approach by pigeons when landing. *J. Exp. Biol.* **180**, 82–104.

Yu, B., Gabriel, D., Noble, L. and An, K. N. (1999). Estimate of the optimum cutoff frequency for the Butterworth low-pass digital filter. *J. Appl. Biomech.* **15**, 318–329.

Appendix B

Supplemental information - Mallard landing approach kinematics driven primarily by horizontal impact velocity

Code repository

Python code to analyze extracted kinematic parameters on landing waterfowl through general linear models and principle component analysis to describe the kinematics and behavioral trends within the data

https://github.com/TheSochaLab/Mallard-landing-approach-kinematics-driven-primarily-by-horizontal-impact-velocity

B.1 *Construction of a Rotational Stereo Videography (RSV) rig*

The rotational stereo videography (RSV) rig was developed by de Margerie et al. (2015) and enables the tracking of a subject from a distance through a single telescopic lens. An array of mirrors reflects the subject back to the camera creating a split screen, which allows 3D reconstruction and tracking in the field. A diagram of the version developed from their methods for tracking mallards' landing behavior is shown below.

First surface mirrors

First surface mirrors were used for the RSV rig. This type of mirror make alignment and focus of the images the camera clear and consistent. A first surface mirror has the reflective surface on the front of the glass, not behind as is more typical of mirrors used in the home. As a result, light hitting a first surface mirror does not refract multiple times through a pane of glass to reach then reflect off of the reflective surface. Thereby allowing the construction of a mirror array to be done with greater consistency and generate a clearer image. As a result, first surface mirrors are commonly used in scientific instruments such as telescopes and microscopes. However, they are not readily used everywhere because the reflective surface is

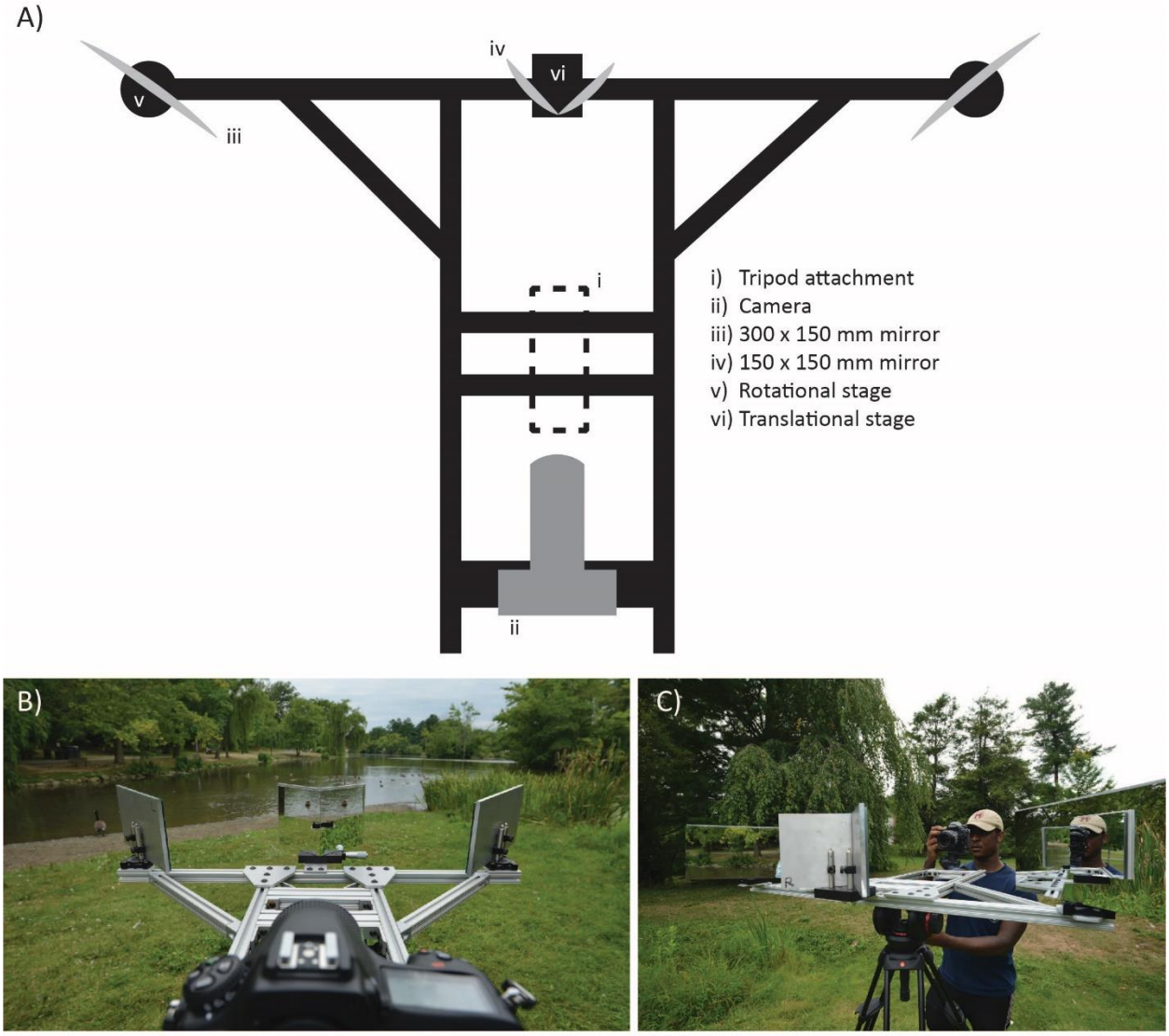

Diagram of how the rotational stereo videography (RSV) rig is constructed (A). The perpective when looking down the rig (B) and Ira Moore prepared to record with the RSV rig (C). When tracking, it is easiest to look over the top of the camera (B) and place the subject at the verticies of the top of the two smaller mirrors so the recorder is looking directly at the subject and not a reflection. This allows reliable recording of the ducks without having to watch the LED screen on the camera, which limits the ability of the tracker to see ducks approach and anticipate their position. The recorder should also use the position demonstrated by Ira (C), left hand controlling the tripod and right hand on the camera. This positioning enables the recorder to pan the rig while simultaneously triggering recording. The hand on the camera should be very light, its sole function is to trigger recording. The rig can be panned using just a hand on the camera, but sharp movements can shift the camera position. Therefore, it is best to not put any pressure on the camera and simply trigger recordings. When panning, it is easiest to keep your body square with the rig and gradually twist your upper torso with the rig. This will limit sudden sharp movements with the rig and make it easier to keep a line of sight on the subject in the verticies of the mirrors.

exposed and easily damaged. For the handling and maintenance of first surface mirrors the following was done. Mirrors were always handled with nitrile or latex gloves and experimenters actively avoided touching the reflective surface. When packaging the RSV rig the mirrors were stored in a hard case and surrounded by foam. In addition, each mirror had the reflective surface protected with Kim wipes. The wipes were taped to the aluminum plate back of the

mirror so the wipes wrap around to hang in front of the reflective surface. mirrors to protect them from becoming scratched by the foam. Great care was taken to prevent debris landing or accumulating on the surface of the mirror as it is best not to clean them. If debris did fall on a mirror in the field the mirror would be inverted to see if the debris will fall off. If it would not, the experimenter could lightly blow on the region to see if the debris could be dislodged. If not, the debris was left alone to be dealt with in lab. In lab the mirror would be soaked in water to dislodge the debris and dabbled dry with Kim wipes. As a rule, do not wipe or press firmly upon the reflective surface to clean it, it is liable to scratch. Also, do not clean the mirror with Windex or any other ammonia-based glass cleaner, it may break down the reflective surface. When not in use, these mirrors should always be stored in a hard case, to prevent contact with other surfaces, but also to prevent dust accumulation which would require cleaning.

B.2 *Recording and calibration of RSV rig*

As with the GoPro array the RSV rig required a calibration and the same wand method was used. However this wand was smaller, 29 cm in length, on the end of a meter-long rod to prevent hands and arms from blocking digitization of the wand points. An experimenter would lock the RSV rig tripod in place and start the recording. A second experimenter would stand approximately 25 meters away and hold the end of the wand furthest away from the digitization points lightly in two fingers and let the wand come to rest, creating a dipole. Again, once the wand stopped swaying this position was maintained for a count of 10. Then, the experimenter with the wand would walk towards the rig while slowly moving the wand in circles. No synchronization methods were used with the RSV as the recording is a split screen on the same camera so the perspectives are inherently synchronized. All recordings from the RSV were saved following the same format as for the GoPro array (A.1) except instead of ‘GP’ denoting the recording occurred with GoPro’s the filenames have ‘RSV’ denoting they were recorded on the RSV.

B.3 *Processing of videos and digitization of points*

Video processing of RSV videos followed the same workflow as used for the GoPro array.

Catalog and matching of videos

Videos were downloaded into folders based on date, catalogued, and clipped into shorter videos of the individually tracked landings, which were labeled using the same filename system, “[YYYYMMDD]-RSV.[‘Calib’ or ‘Landing’].[A-Z][01-99][a-z]”. Camera is not included in this filename as all come from the same camera and there is one video. In addition, the landings recorded in the RSV were matched to the corresponding landings from the perspective of the GoPro’s. This matching was done by timestamp followed by sequence order and the matching of the position of the proximate waterfowl seen in the RSV footage and GoPro’s.

Video processing and digitization

Once the landings and corresponding calibration videos had been identified, all the relevant videos were de-warped and digitized in Argus in the same way as the GoPro's with two exceptions. One, the Pattern feature of Argus (Jackson et al., 2016) was used to find the distortion coefficients of the 105 mm lens and D80 Nikon camera used for the RSV. Two, no synchronization was done with Argus' Sync as the videos are inherently synced.

When digitizing the wands and the points on the duck in Clicker there is an additional adjustment to the workflow. There is only one video after all the processing, but you need at least two as Clicker will not except a repeat video file. Therefore, before digitization of a calibration or landing video the file is duplicated and a '-L' and '-R' is appended to the end of the filenames. During digitization the left hand side of the video (since you always see both) is always digitized in the '-L' video and the right hand side of the video is always digitized in the '-R' video. Wand points were digitized by skipping forward frames and ensuring at least 100 wands using the same method as for the GoPro videos. The wand was digitized from the start of the wand carrier walking forward until they have gone 3 steps forward. This creates a volume of interest (VOI) that is approximately 1 m^3 around 20 meters from the RSV rig, which corresponded to the distance to the primary landing area on the pond from the rig.

Multiple features on the mallards were digitized: tip of the bill, base of the bill, shoulder (where wing meets the body), the tip of the wing, breast (where neck plumage changes color - only digitizable on males), base of the a tail (defined as where line of white tail feathers stop upon merging with the body), tip of the tail, heel (base joint of foot), and toe (longest toe, digit 3). Digitization of all these points were attempted for recorded landings. During digitization a catalog was created specifically for the RSV digitization. This catalog included the frames at which the feet were extended, the feet impact the water, the breast impacts the water, and the tail wag or flip at the end of a skim occurs. In addition, to these frames the start and end frames for each point on the body being digitized was recorded and landing identification information, e.g. date and video label. However, most body points could not be digitized reliably. Those that were consistently available for digitization were the shoulder, base of tail, tip of tail, base of bill, and tip of bill.

B.4 *Code for analysis of kinematic data*

All the 3D points from the tracking were imported into Python to be interpolated and filtered. The points digitized on the mallards were rearranged before further analysis. The data import as 30 columns for each landing, 3 columns for each of the 10 body parts digitized. The data for a given landing was split into columns based on body part and stacked as landings separately, but in the same order. Once organized all data was clipped based on frame values from the catalog for the start and end of digitization for body part.

Cubic spline interpolation, frame of reference standardization, and Butterworth filter

Some of the digitization had gaps which were interpolated by a cubic spline, through Pandas `interpolate`, along each of the three axes

$$\overrightarrow{x_i}(t) = \overrightarrow{a_i} + \overrightarrow{b_i}t + \overrightarrow{c_i}t^2 + \overrightarrow{d_i}t^3 \quad \text{(B.4.1)}$$

$$\overrightarrow{y_i}(t) = \overrightarrow{a_i} + \overrightarrow{b_i}t + \overrightarrow{c_i}t^2 + \overrightarrow{d_i}t^3 \quad \text{(B.4.2)}$$

$$\overrightarrow{z_i}(t) = \overrightarrow{a_i} + \overrightarrow{b_i}t + \overrightarrow{c_i}t^2 + \overrightarrow{d_i}t^3 \quad \text{(B.4.3)}$$

This allows us to fill in the gaps in the data so that $\overrightarrow{p_i} = [\overrightarrow{x_i}(t), \overrightarrow{y_i}(t), \overrightarrow{z_i}(t)]$ where t for a given axis was a parameter limit defined by the following

$$\overrightarrow{x_i}(0) = \overrightarrow{p_i} \quad \text{(B.4.4)}$$

$$\overrightarrow{x_i}(t_i) = \overrightarrow{p_i} + 1 \quad \text{(B.4.5)}$$

$$\overrightarrow{\dot{x}_i}(0) = \overrightarrow{m_i} \quad \text{(B.4.6)}$$

$$\overrightarrow{\dot{x}_i}(t_i) = \overrightarrow{m_{i_1}} \quad \text{(B.4.7)}$$

To account for the actual position, p_i, and the tangent vectors for each position, m_i. The vector coefficients for the spline: a, b, c, and d, are calculated as

$$\overrightarrow{a_i} = \overrightarrow{p_i} \quad \text{(B.4.8)}$$

$$\overrightarrow{b_i} = \overrightarrow{m_i} \quad \text{(B.4.9)}$$

$$\overrightarrow{c_i} = \frac{3(\vec{p}_{i+1} - \vec{p}_i)}{t_i^2} - \frac{2\overrightarrow{m_i} + \overrightarrow{m}_{i+1}}{t_i} \quad \text{(B.4.10)}$$

$$\overrightarrow{d_i} = \frac{2(\vec{p}_{i+1} - \vec{p}_i)}{t_i^3} - \frac{\overrightarrow{m_i} + \overrightarrow{m}_{i+1}}{t_i^2} \quad \text{(B.4.11)}$$

A cubic spline was used to interpolate the gaps in this case as opposed to a Kalman filter because the frame of reference changes during filming due to the panning of the RSV rig. Therefore, the position points do not necessarily follow a predictive path based on the previous velocity and acceleration. Once the gaps were interpolated the data was translated to have a constant frame of reference.

This constant frame of reference was defined as the midpoint between the shoulder and base of tail. This point was chosen because the distance between the shoulder and base of tail must be constant. A duck's spine has a number of fused vertebrae along the back including the synsacrum at the hip joints which help it maintain a level posture in flight. However, this also means the bird cannot effectively bend this region of its body and therefore the distance between the shoulder and base of tail cannot change during landing. Once the midpoint was calculated for all frames in which both the shoulder and base of tail were digitized, all other data was truncated to correspond with this time frame, enabling all points to be translated so that the midpoint of the mallard is the origin in all frames. Last, the translated data of each

body point was filtered with a Butterworth (A.3.11) with a frequency range for cutoffs of 1 – 35 Hz at 0.5 Hz increments with a 95% cutoff (Yu et al., 1999).

Extraction of body angle and transition duration

Body angle was calculated based on the positions of the base of the tail and the position of the shoulder. To find this angle the base of tail is turned into the origin and the shoulder is translated accordingly. Then, a second hypothetical point is created that is parallel to the water surface by placing it at the height of the base of the tail, zero, and underneath the shoulder in space. Once this hypothetical point exists, b, the angle relative to the origin can be calculated with the point at the shoulder as a.

$$\cos\theta = \frac{a \cdot b}{|a||b|} \tag{B.4.12}$$

Once the angle of the body was calculated for a landing, the value at the moment of initial impact, e.g. when the feet hit the water, was extracted. This value is assumed to be representative of the range of body motion during the transition as all landings eventually end with the duck horizontally buoyant on the surface of the water. Detailed measure of this angle throughout the transition could not be assessed due splash during impact which prevents the digitization of the base of the tail soon after impact.

Transition duration was calculated based on the number of frames, n_f, between initial impact and the impact of the breast on the water multiplied by the frame rate of the recording

$$t_{trans} = {}^{n_f}/_{119.97\ sec^{-1}} \tag{B.4.13}$$

Both body angle and time duration are appended onto a combined data catalog which merges the landing data from the GoPro array and the RSV rig enabling kinematic analyses of landing with data from both camera systems.

General linear regression model

For analyses the following kinematic parameters were extracted: impact speed, horizontal impact velocity, vertical impact velocity, impact angle, mean approach angle, distance after impact, body angle, and transition duration.

To assess the relationship of the various kinematic parameters to distance after impact a general linear model (GLM) was created using Python `StatsModels` package. However, to carry out a GLM, the variance inflation factors (VIF) for the variables must be compared.

$$VIF_i = \frac{1}{1-R_i^2} \tag{B.4.14}$$

These VIF values give a measure of how much collinearity there is between the variables you are using. There are rules of thumb for what degree of collinearity is too high, which is typically 10, but people also recommend concern for any value over 5. However, the reason for theses

rules is that if there is a high degree of collinearity between variables in a multiple regression analysis it can confound the results (O'Brien, 2007). For instance, GLM may show significant changes in the coefficients and p-values reported for the tested variables with the exclusion or inclusion of one of the variables. This behavior is indicative of variable with high collinearity to the others and it is changing the result. If a GLM is working correctly, the coefficients and p-values should remain relatively constant regardless of the addition or loss of variables.

The VIF for vertical impact velocity, horizontal impact velocity, impact angle, and mean approach angle are high, with values of 28, 5, 14, and 4 correspondingly. However, when you exclude vertical impact velocity (highest level of collinearity) from the analysis the collinearity drops to 2, 3, and 4 for horizontal impact velocity, impact angle, and mean approach angle. This suggests that vertical impact velocity has an incredibly high degree of collinearity with the other three, and while the other three parameters still have significant collinearity between them it is at an acceptable level unlikely to cause issues for a multiple regression analysis. Therefore, a GLM is reasonable for modeling horizontal impact velocity, impact angle, and mean approach angle to distance after impact. Yet, that does not mean vertical impact velocity must be ruled out of the analysis. If the inclusion of vertical impact velocity does not shift the results of a GLM for the other three parameters, it is likely that collinearity observed in vertical impact velocity is not causing an error in the model. Therefore, two GLM's were run.

More information is still needed before those GLM's can be run. First, the residuals of the dataset were plotted using `Stats ProbPlot` and found them to follow a gamma distribution. In addition, the trends between the approach kinematics and distance after impact are all a better fit for exponential or logarithmic and a GLM assumes linearity. Therefore, the family of GLM for these analyses was gamma and the model had logarithmic link to make the relationships more linear. Both GLMs were then run; once on all four parameters and once on all but vertical impact velocity.

$$\eta_i = \beta_0 + \beta_1 x_{1i} + \beta_2 x_{2i} + \beta_3 x_{3i} + \beta_4 x_{4i} \quad \text{(B.4.15)}$$

$$\eta_i = \beta_0 + \beta_1 x_{1i} + \beta_2 x_{2i} + \beta_3 x_{3i} \quad \text{(B.4.16)}$$

Where β_n are the various coefficients and x_{ni} are the variables. The results of both these models show that the coefficients and p-values for horizontal impact velocity, impact angle, and mean approach angle are the same with or without vertical impact velocity. Therefore, despite the high collinearity vertical impact velocity was included in this analysis.

Principle component analysis

To examine the key kinematics a principle component analysis (PCA) was run. The goal was to examine if the collinearity inherent between horizontal impact velocity, impact angle, and mean approach angle are suggestive of any landing types or behaviors. The `SciKit-learn` Python package was utilized to carry out the analysis. Within this package there is both a

`StandardScaler` kit and a `PCA` kit. `StandardScaler` uses the standard score, z, to normalize a dataset

$$z = \frac{(x-\mu)}{\sigma} \tag{B.4.17}$$

Where x is the sample, μ is the mean, and σ is the standard deviation. With the data standardized based on variation from the mean it can be used for a PCA, which will find the major axes of variation within the dataset. The weights, explained variation per principal component, were 0.7, 0.23, and 0.06 from component one to three.

K-cluster algorithm

A K-cluster algorithm detects centromeres, clusters of data that are more closely related to each other than others. Using the `SciPy Cluster` package a k-cluster was run upon the results from the PCA analysis. The first step of a clustering algorithm is identifying the correct number of clusters. This was done through the 'elbow' method, which looks at the mean variance found for the data when grouped into different numbers of centromeres. The number of groups at which the variance 'elbows', begins to flatten toward an asymptote on the x-axis is the most likely number of clusters within the dataset. For this analysis the 'elbow' occurs at 2 groups, therefore 2 is the number of centromeres assumed to be present in the dataset. The algorithm then calculates the position of the two centromeres, the distance of all each data point to each centromere, and assigns each point to a group or cluster based on which mean it is closest to.

B.5 *References*

de Margerie, E., Simonneau, M., Caudal, J.-P. P., Houdelier, C., and Lumineau, S. (2015). 3D tracking of animals in the field using rotational stereo videography. *J. Exp. Biol.* **218**, 2496–2504.

Jackson, B. E., Evangelista, D. J., Ray, D. D. and Hedrick, T. L. (2016). 3D for the people: multi-camera motion capture in the field with consumer-grade cameras and open source software. *Biol. Open* **5**, 1334–1342.

O'Brien, R. M. (2007). A caution regarding rules of thumb for variance inflation factors. *Qual. Quant.* **41**, 673–690.

Yu, B., Gabriel, D., Noble, L. and An, K. N. (1999). Estimate of the optimum cutoff frequency for the Butterworth low-pass digital filter. *J. Appl. Biomech.* **15**, 318–329.

Appendix C

Supplemental information – Mallards avoid obstacles when landing on water

Code repository

Python code to process 3D position of other waterfowl with respect to the landing mallards, analysis of proximity data, and simulations to test randomization within the landing behavior

https://github.com/TheSochaLab/Mallards-avoid-obstacles-when-landing-on-water

C.1 *Procedure for digitization of waterfowl on surface of the pond*

To digitize the other waterfowl that were proximate on the pond Argus' Clicker (Jackson et al., 2016) was used. Each landing event was imported into Clicker in ascending order, synchronization values were input based on the digitization catalog, and the corresponding calibration direct linear transformation coefficients were uploaded. Then, auto-advance was turned off and the frame of initial impact was selected. Each waterfowl that was swimming in the water, regardless of species, was digitized as a separate track for the impact frame of each landing. Argus does not allow multiple points in the same frame for a single track. Once all waterfowl who could be seen in at least two cameras were digitized the four corners on the bench across the cove were digitized as was the position of the feeder (individual feeding ducks) if they were present. Digitization files were exported with the standard format, but with the addition of 'consp' after 'digi' to denote that it's a digitization of conspecifics: "[YYYYMMDD]-digi-consp-GP. Landing.[A-Z][01-99][a-z]".

C.2 *Proximity analysis*

For the proximity analysis all proximity data in 3D and the digitization catalog from the trajectory data, which includes all parameters calculated in parts A and B of these appendices, were uploaded to Python. However, the catalog also has two additional parameters calculated for the proximity analysis: landing direction angle and the deviation from that angle by the end of a skim. Landing direction was found based on the 3D trajectory data and based on v_x and v_y to calculate the yaw angle at impact, γ_{imp}

$$\gamma_{imp} = \tan^{-1}(v_y/v_x) \quad \text{(C.2.1)}$$

To find the angle of deviation from the landing direction the difference in the x and y axes for position of duck was found between the moments of impact to the end of a skim, making the origin for the angle initial impact. The angle, γ_{end}, was then calculated

$$\gamma_{end} = \tan^{-1}(y/x) \quad \text{(C.2.2)}$$

Then, to account for quadrant, if the resulting angles for both γ_{imp} and γ_{end} were positive or negative, γ_{end} was subtracted from γ_{imp}. If they have opposite signs they were simply added together. Last, the absolute value of the difference between the angles was taken to find the magnitude of the difference. With these two additional measurements from the trajectory data in the catalog all remaining analyses can be done with only the catalog and proximity positions.

In analyzing the proximity data, the first step was to simply count how many waterfowl were in the area for each landing event by putting all individuals position coordinates into an array. The length of the array would then inform you of the number of individuals. Next, all points are translated based on the position of initial impact, making initial impact the origin. At which point the distance of each individual can be calculate based on the hypotenuse of their x and y coordinates.

$$d = \sqrt{x^2 + y^2} \quad \text{(C.2.3)}$$

With this information the number of individuals within the landing area and strip can be tested. The number within a landing area was simply found by finding the number of individuals for each landing event that are less than the maximum skim distance from the position of impact, 6.02 m. The number of individuals in a landing strip was found based on whether the distance to impact was less than 6.02 meters and if the angle between that individual and the position of impact, φ, was greater than the minimum range of landing direction angle plus and minus the standard deviation of deviations from landing direction.

$$\varphi = \cos^{-1}\left(x/d\right) \quad \text{(C.2.4)}$$

C.3 *Simulation analysis*

To simulate landing events randomly, `Pandas` and `Numpy` packages in Python were used. For each iteration of the randomized heading simulation `numpy.random.randomint` was used

to generate a new heading for each landing event. This angle was then analyzed for position within the landing area and landing strip just as the actual data had been. The shuffle simulation was similar, except instead of a new dataset of random heading for each iteration the `DataFrame.sample` command was used to re-select a new header from the dataset for each landing event. Thereby creating a shuffled dataset with regards to heading direction for each iteration.

C.4 *References*

Jackson, B. E., Evangelista, D. J., Ray, D. D. and Hedrick, T. L. (2016). 3D for the people: multi-camera motion capture in the field with consumer-grade cameras and open source software. *Biol. Open* **5**, 1334–1342.